공학석사 학위논문

Shock Response Analysis of Chamber Model under Internal Blast

모형 체임버의 내부폭발 내충격 응답해석

지도교수 이 상 갑

2017 년 2 월

한국해양대학교 대학원

조선해양시스템공학과

이 환 수

본 논문을 이환수의 공학석사 학위논문으로 인준함.

위원장	박 석 주	(인)
위 원	이 상 갑	(인)
위 원	남 종 호	(인)

2017 년 2 월

한국해양대학교 대학원

Table of Contents

List of Tables

List of Figures

모형 체임버의 내부폭발 내충격 응답해석

이 환 수

한국해양대학교 대학원
조선해양시스템공학과

초 록

함정 격실 내부폭발 시 함정의 생존성 향상을 위하여 손상구역을 제한하여야 하며 함내 인접격실로의 피해확산 방지 및 연속적인 침수 억제를 위하여 폭발강화격벽 (BHB: Blast Hardened Bulkhead)의 설계 및 성능검증 기술 개발이 필요하다. 본 연구에서는 내부폭발에 의한 폭발강화격벽의 거동평가 기술을 개발하기 위하여 LS-DYNA code의 MMALE (Multi-Material Arbitrary Lagrangian Eulerian) 및 FSI (Fluid-Structure Interaction) 해석기법을 이용한 폭발강화격벽 및 연결부 거동의 내부폭발 내충격 응답해석 기술을 개발하였다. 본 연구에서는 축소 및 부분모형 체임버의 격벽의 내부폭발 시험에 대하여 내부폭발 내충격 응답해석을 수행하여 거동 해석기법을 검증하고 격벽 모델의 내충격 응답특성도 파악하였다.

1. Introduction

It is necessary to develop design guidance and performance verification technique of Blast Hardened Bulkhead (BHB) in naval ship for restriction of Explosion Resistance (ER) zoning to a one section for the enhancement of ship survivability under the internal blast of Semi-Armor Piercing (SAP) warhead inside the compartment of naval ship, as shown in Figs. 1 & 2. BHB was already developed and has been applied to the naval ship in some countries (Galle & Erkel, 2002; Stark & Sajdak, 2012), and has been partially adopted into some navy ships with the foreign techniques.

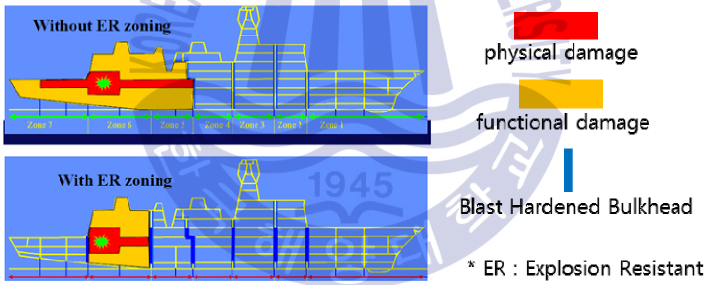

Fig. 1 Zoning of Explosion Resistance (ER) through adoption of Blast Hardening Bulkhead

Fig. 2 Internal explosion damage of USS Stark (FFG-31) by Exocet Missiles (Raymond, 2001)

Diverse scale internal blast tests of BHB were carried out, and its design and analysis techniques were also verified for its application abroad. TNO carried out full scale internal blast test of BHB through the internal blast test using retired naval ship (Galle & Erkel, 2002), as shown in Fig. 3, and DSTO, also, internal blast test of part transverse bulkhead model of real one, as shown in Fig. 4(a), and investigated its shock response and factors related to the design constraints (Raymond, 2001). Diverse scale internal blast tests were performed using real scale compartment of naval ship, etc., as shown in Fig. 4(b), in the USA.

Fig. 3 Internal blast test of retired ship and BHD model by TNO (Galle & Erkel, 2002)

(a) part model by DSTO (b) real scale in USA

Fig. 4 Internal blast test of part model by DSTO (Raymond, 2001) and full scale bulkhead model in USA.

For the self-development of BHB, its effective analysis, design and verification techniques are needed based on the full scale internal blast test. Structural behavior evaluation technique under the internal blast is necessary to reduce the cost and time for the BHB design, and to estimate the exact response behavior according to design pattern and size, through the prediction of diverse behaviors according to the BHB design by the numerical simulation instead of explosion test. Multi-Material Arbitrary Lagrangian Eulerian (MMALE) formulation and Euler–Lagrange coupling algorithm of LS-DYNA code (LSTC, 2013), as shown in Fig. 5, were used for the development of shock response analysis technique of BHB under the internal blast.

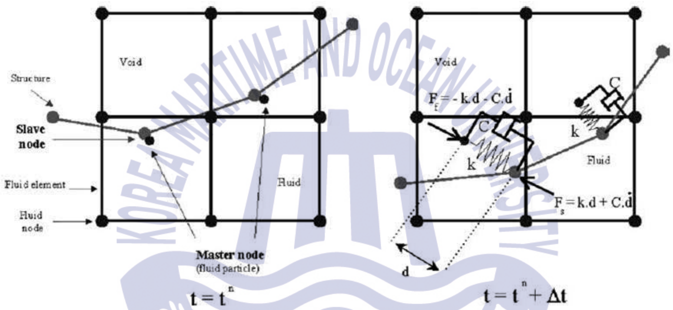

Fig. 5 Sketch of Penalty Coupling Algorithm (Aquelet, et al., 2006)

In this study shock response analysis of 5 bulkhead models was carried out for the internal blast test of reduced scale chamber as the basis research for the real scale blast test, structural behavior analysis technique was verified, and their shock response characteristics was also figured out. At the next step, response analysis of real scale partial chamber model with 2 bulkhead models and several stand-off distances was performed and compared with test results for the internal blast test based on the reduced scale chamber test and response analysis results.

2. Internal Blast Test of Chamber Models

Reduced scale and partial chamber models are largely consisted of chamber, bulkhead structure and clamp frame, as shown in Figs. 6 & 7, with the ratio of chamber dimension as 2.0 : 1.0 : 0.75 by its length, breadth and height, and the dimension ratio of reduced scale and partial ones as 1.0 : 0.25. Detachable bulkhead structure was replaced in every test, and was compressed by the wedges between cartridge and clamp frames for the protection of explosion shock pressure leakage between chamber and bulkhead cartridge. Measuring gauges were attached on the bulkhead and measured for the pressure, acceleration and strain responses under the internal blast test, as shown in Figs. 6(b) & 7(b).

(a) front view w/o bulkhead (b) front view w/ bulkhead

(c) rear view w/ opening (d) iso view of chamber test model

Fig. 6 Reduced scale chamber model for internal blast

(a) front view w/o bulkhead

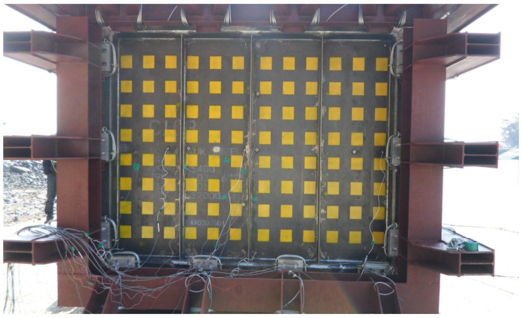

(b) front view w/ bulkhead

(c) rear view w/ opening

(d) iso view of chamber model

Fig. 7 Partial chamber model for internal blast test

In reduced scale chamber test model, bulkhead plate and stiffeners were welded to the inserted plate, as shown in Fig. 8(a) & (b), and the whole inserted plate was contacted to the inside of cartridge frame and attached by spot welding along its center line, as shown in Fig. 8(c). Cartridge frame was manufactured by welding two SQ pipes partially. In partial chamber, bulkhead was installed inside the SQ pipe type cartridge with three stiffeners. Mild steel (SS41) was used for whole parts of two types of chamber models, except the bulkhead and stiffeners of partial chamber with high tensile steel (AH36).

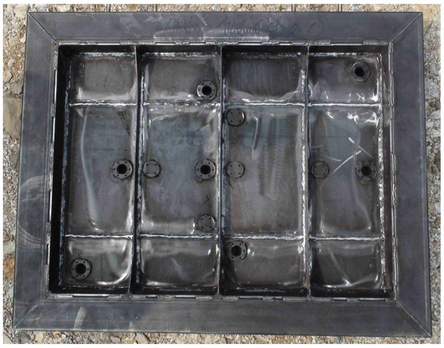

(a) front side

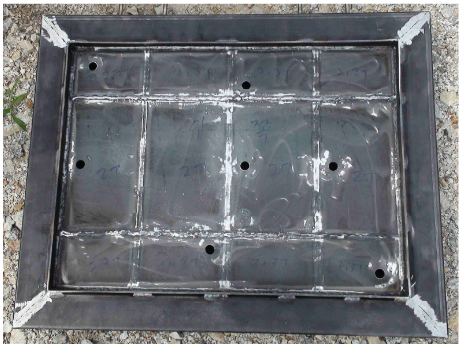

(b) back side

(c) spot welding in inserted plate

Fig. 8 Reduced scale bulkhead model

Table 1 summarizes the general information of 5 bulkhead models, such as curtain and plain bulkhead plate type, the number of side welding edge of bulkhead and inserted plate, the number of basic and auxiliary stiffeners, welding type between sponson part of inserted plate and cartridge frame. Figure 9 shows the schematic diagram of bulkhead according to the number of side welding edge. Bulkhead models 1~3 were used for the first internal blast test, and bulkhead models 4~5, for the second one. High explosive (HE) and low explosive (LE) TNT charges were used for each chamber model, where the ratio of HE and LE TNT charge was 1.0 : 0.075

Table 1 Information of 5 bulkhead models of reduced scale chamber model

model	BH type	No. of side welding edge	No. of BH stiffeners	welding type bt. inserted plate & cartridge
1	curtain	4	3	partial
2	plain	4	3	partial
3	plain	3	3+1(auxiliary)	partial
4	plain	4	3+2(auxiliary)	continuous
5	plain	2	5	continuous

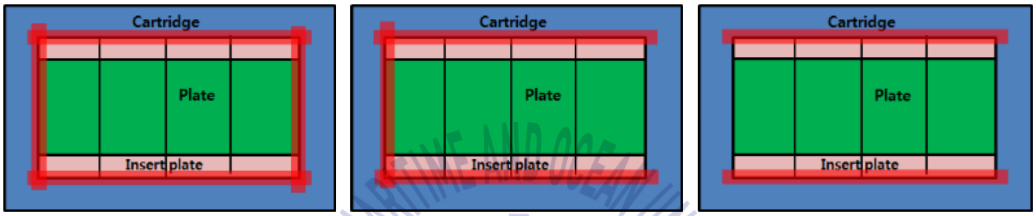

(a) 4 edge (b) 3 edge (c) 2 edge

Fig. 9 Schematic diagram of bulkhead according to welding edge

Two types of bulkheads, such as plain and curtain types, were considered for the internal blast test of partial chamber model, as shown in Table 2. The ratio of HE and LE TNT charges was also 1.0 : 0.075, as the reduced scale chamber model, however, their TNT charge ratio was 1.0 : 0.0156 between reduced scale and partial bulkhead models. Internal blast test and shock response results of HE and LE TNT charges were considered and compared with each other. Three stand-off distances, such as L/2, L/4 and L/8, were typically considered for the shock response characteristics and plastic deformation of plain plate type bulkhead, where L stands for the chamber length. Curtain plate type bulkhead was also considered at stand-off distance together with reversed direction of bulkhead, as shown in Table 2. The last test was the close internal blast one for the fracture criterion of bulkhead material and welding effect with double HE TNT charge.

Table 2 Information of 2 bulkhead models of partial chamber model

Model	Bulkhead type	Location of explosive	Type of explosive	Direction of bulkhead	No. of test
1	plain	L/2	HE TNT	normal	3 & 6
2	plain	L/4	HE TNT	normal	4
3	plain	L/8	HE TNT	normal	2
4	plain	L/2	LE TNT	normal	1 & 5
5	curtain	L/2	HE TNT	normal	9
6	curtain	L/2	HE TNT	reversed	10
7	plain	L/16	2 × HE TNT	normal	11

Damage configurations of 5 reduced scale chamber bulkhead models are shown in Fig. 10 under internal blast test. It could be found that damage response of bulkhead structure with relatively thin plate, 2.0mm, was very sensitive to the welding effect. These characteristics were suitably realized by modeling for the internal blast response analysis. As the bulkhead was bent outward, outside inserted plate contacted to the cartridge was also bent outward and was integrated to the cartridge. Since the sponson part of inside inserted plate was also bent inward, its sponson part was detached or attached according to their partial and continuous welding condition to the cartridge.

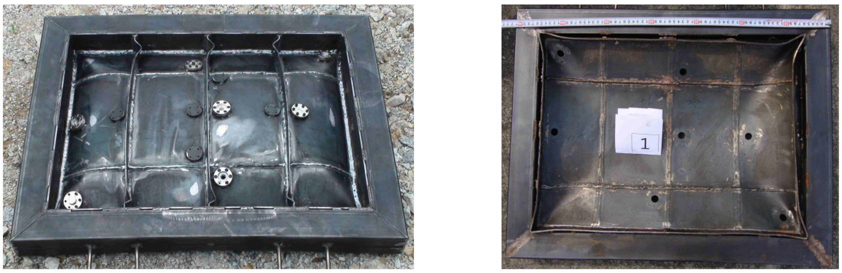

(a) 1st model

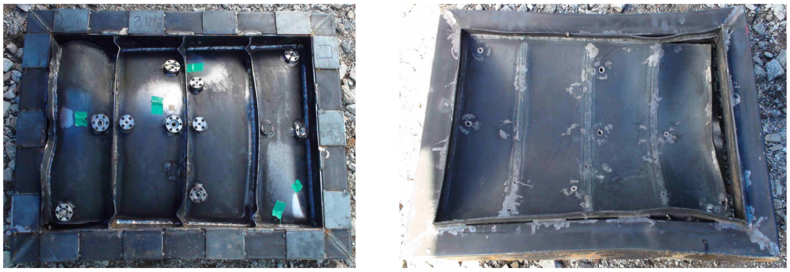

(b) 2nd model

(c) 3rd model

(d) 4th model

(e) 5th model

Fig. 10 Damage configurations of reduced scale chamber bulkhead models under internal blast test

Figure 11(a) & (b) shows the damaged configuration of plain type bulkhead and curtain type one with reversed direction at stand-off distance, respectively. The every end of stiffeners was only torn away in the curtain plate type bulkhead with reversed direction in this blast test of partial chamber model. The fracture at the end of stiffener occurred at the location right off the welding bead, not at the welding line. The bead thickness was considered in the shock response analysis. For the establishment of fracture criterion in partial chamber bulkhead model, very close internal blast test was carried out, where the whole bulkhead was torn away from the bulkhead bead attached in cartridge and most upper and bottom cartridge part, also, along the bulkhead welding line, as shown in Fig. 12.

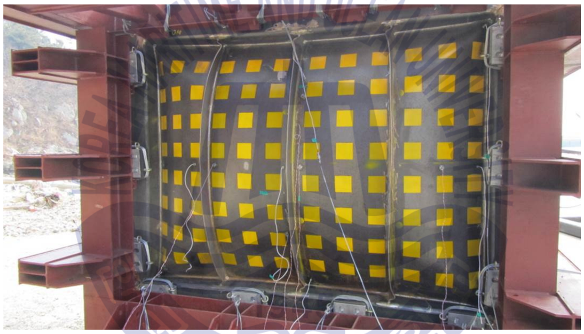

(a) plain plate type BH

(b) curtain plate type BH with reversed direction

Fig. 11 Damage configuration of partial chamber bulkhead under internal blast test at stand-off distance

Fig. 12 Damage configurations of partial chamber bulkhead under internal blast test with 2 × HE TNT at L/16 stand-off distance

3. Modeling of Shock Response Analysis of Chamber Models

Shock response analyses were carried out for reduced scale and partial chamber models by the schedule, as shown in Tables 1 & 2, and their F.E. configurations are shown in Fig. 13, Figure 14 shows the F.E. configuration of air, TNT charge and chamber model according to stand-off distance of TNT charge. Typical TNT charges are shown in Fig. 15, such as spherical type LE & HE in reduced scale chamber model, spherical type LE & HE in partial one, and cylindrical type 2 × HE in partial one. Figure 16 illustrates the bulkhead models of reduced scale and partial chambers, and Fig. 17(a)~(f), 5 bulkhead models of reduced scale chamber. Figure 17(g)~(h) shows the close view of partial chamber bulkhead model, and Fig. 17(i)~(j), additional welding and concrete ones for the internal blast of 2 × HE TNT charge at stand-off distance L/16. MAT_CSCM_CONCRETE option was used for the concrete damage shock response. Shell and solid elements were used for their structures and MMALE of air and charge, respectively, with around 476,000 shell and 2,700,000 solid element numbers for reduced scale chamber model and around 515,000 shell and 8,520,000 solid ones for partial chamber one.

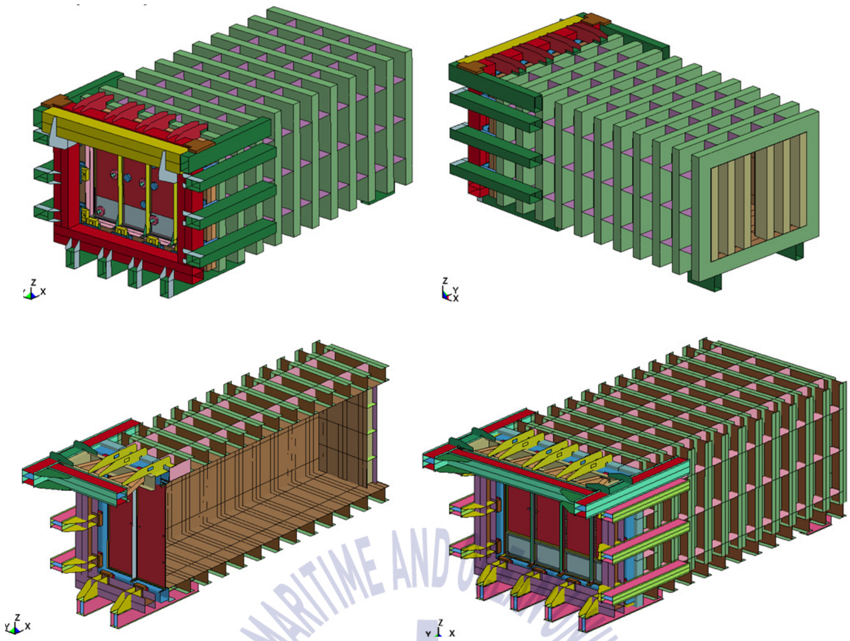

(a) reduced scale chamber model

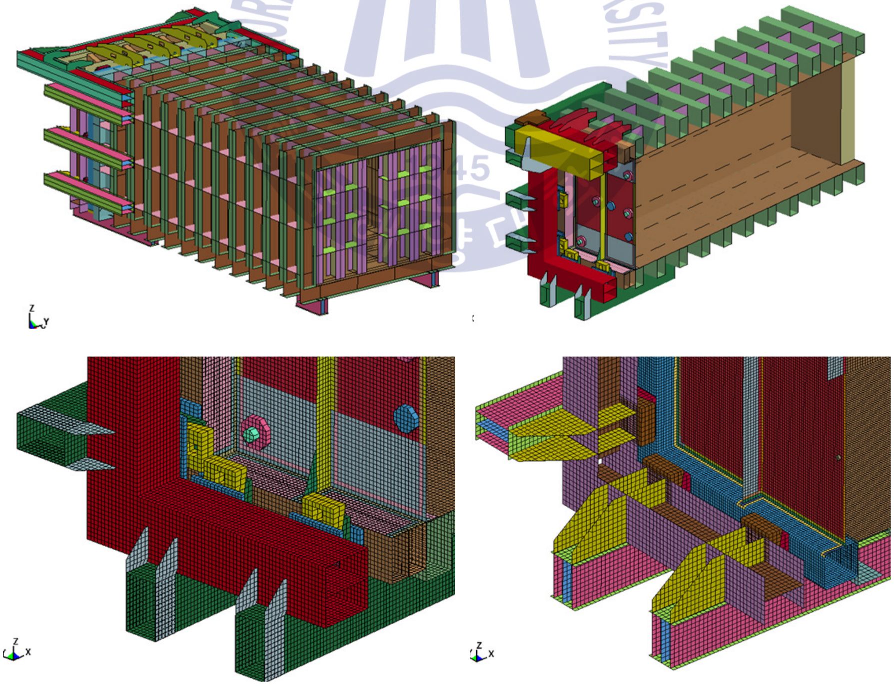

(b) partial chamber model

Fig. 13 F.E. configurations of reduced scale and partial chamber models

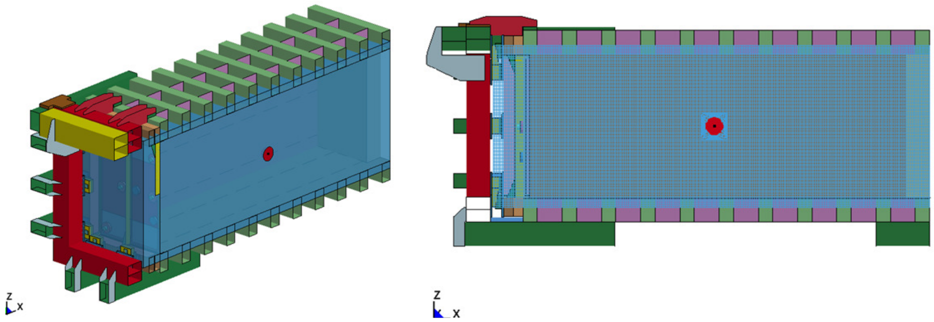

(a) L/2 stand-off distance in reduced scale chamber

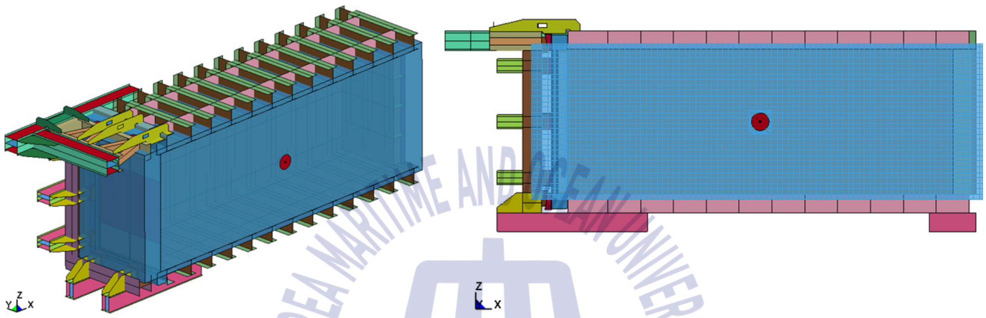

(b) L/2 stand-off distance in partial chamber

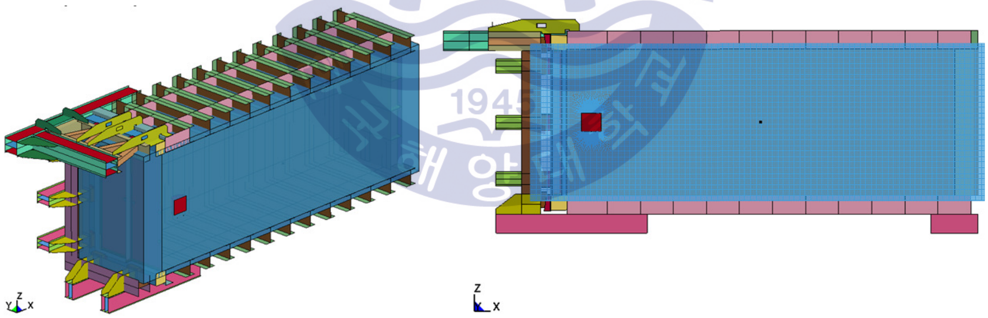

(c) L/16 stand-off distance in partial chamber

Fig. 14 F.E. configurations of air, HE TNT charge and reduced scale & partial chamber models

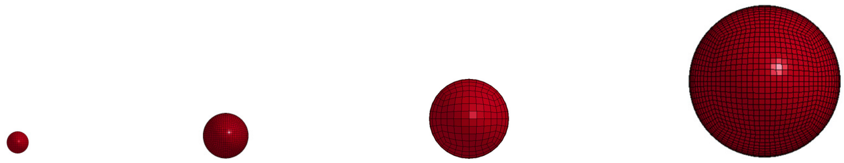

(a) LE reduced (b) HE reduced (c) LE partial (d) HE partial

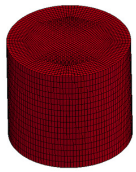

(e) $2\times$HE partial chamber model

Fig. 15 F.E. configurations of TNT charge according to HE & LE, reduced scale & partial chamber, $2\times$HE in partial chamber

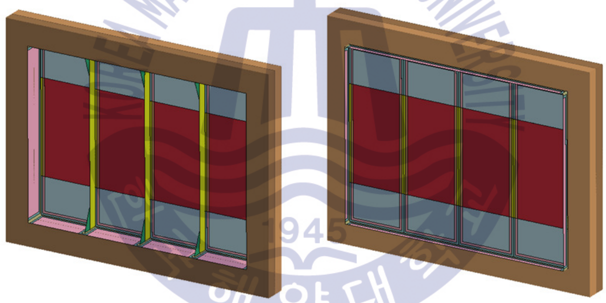

(a) front & back side in reduced scale chamber model

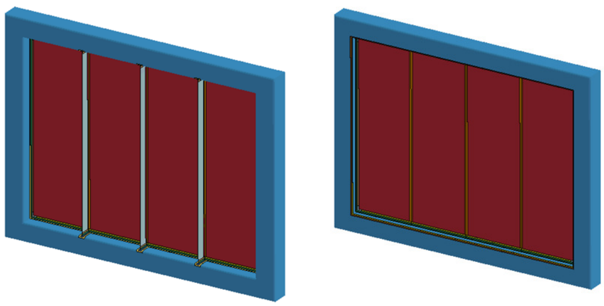

(b) front & back side in partial chamber model

Fig. 16 F.E. configurations of front & back side in reduced scale & partial chamber bulkheads

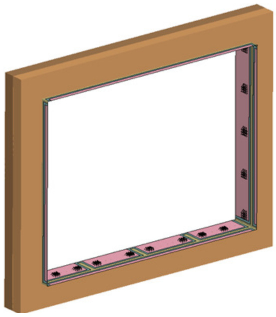

(a) inserted plate & cartridge

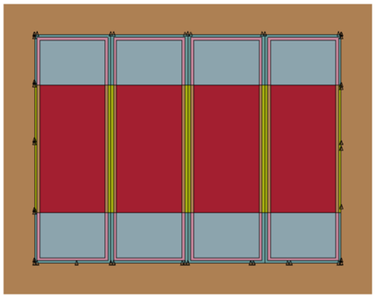

(b) 1st BH (4 edge)

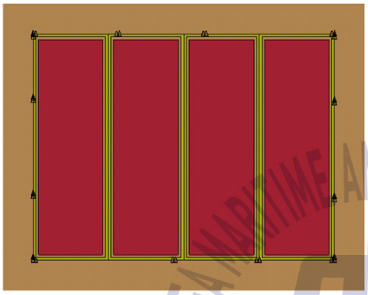

(c) 2nd BH (4 edge)

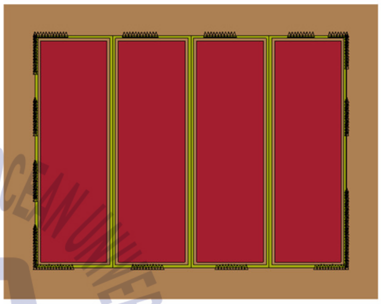

(d) 3rd BH (3 edge)

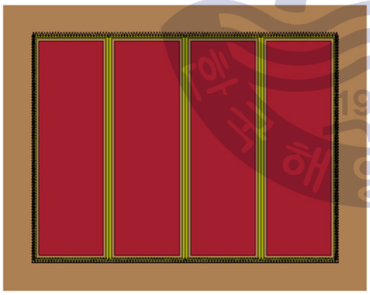

(e) 4th BH (4 edge)

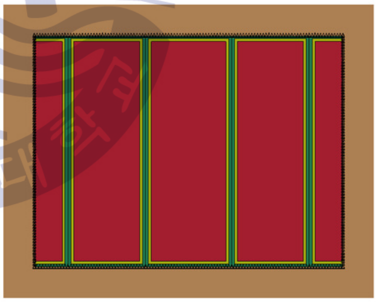

(f) 5th BH (2 edge)

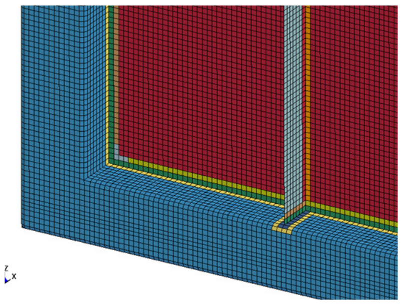

(g) front partial chamber BH

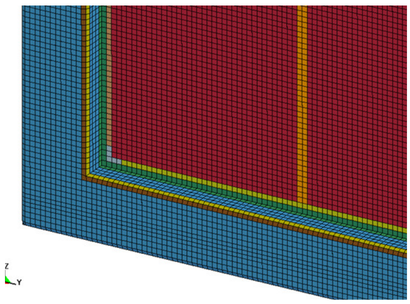

(h) back partial chamber BH

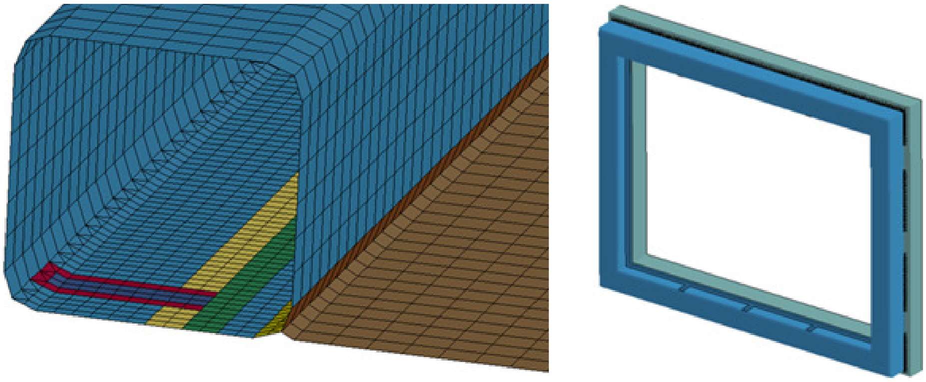

(i) welding along cartridge to chamber and chamber stiffener

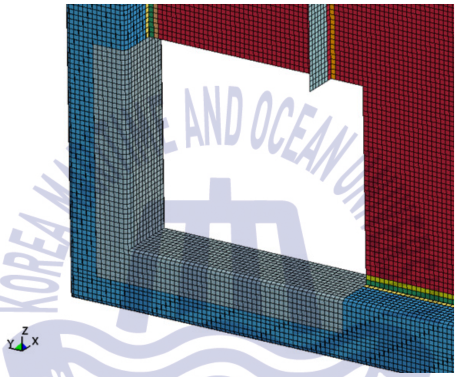

(j) concrete inside cartridge

Fig. 17 F.E. configurations of reduced scale & partial chamber bulkhead considering welding effect

Inserted plate was contacted to the inside of cartridge using CONTACT _SURFACE_TO_SURFACE option, and was welded along the centerline to the cartridge using CONSTRAINT_NODE_SET option, as shown in Fig. 17(a). Partial and continuous welding of the sponson part of inserted plate to the cartridge in reduced scale chamber model was treated by CONSTRAINT_SPOTWELD option, as shown in Fig. 17(b)~(f). Welding effect was treated by increasing the thickness of the welding bead, and by decreasing the failure strain in the neighboring strip near the bead, as shown in Fig. 17(g)~(h). In reduced scale chamber bulkhead, bulkhead was torn away along the bead, since the bulkhead was very thin. Welding line of bulkhead was treated by controlling the failure strain with consideration of the bead thickness. Wedge was pre-stressed and was stuck to the chamber, as shown in Fig. 13. Air ALE solid element was modeled for the surround of the chamber and bulkhead structures, and FSI analysis technique was applied to the air and charge MMALE and chamber and bulkhead structure using CONSTRAINED_ LAGRANGE_IN_SOLID option of LS-DYNA code.

Some stress-strain curves of mild steel (SS41) and high tensile steel (AH36) with short strain range were obtained by the static and high speed tensile test, and curve fitting process was applied to the original ones, as shown in Fig. 18(a). Extended stress-strain curves were suggested for the high strain rate in the case of close internal blast, such as stand-off distance L/16 and $2 \times$ HE TNT charge, using Cowper and Symonds equation, as shown in Fig. 18(b). Their general properties are summarized in Table 3. Shear strain fracture model was adopted for the fracture of structure in the shock response analysis and failure strain was applied to the chamber structure according to the element size to its thickness and welding effect. MAT_PIECEWISE_LINEAR_PLASTICITY (MAT_024) was adopted for the mild and high tensile steels. Pressure and acceleration responses were measured at the locations on reduced scale and partial chamber bulkheads, as shown in Fig. 19.

Table 3 Properties of mild and high tensile steels

Property	Mild steel (SS41)	High tensile steel (AH36)
Young's modulus	206 GPa	206 GPa
Density	7,850 kg/m3	7,850 kg/m3
Poisson’s ratio	0.3	0.3
Mild stress	330 MPa	405 MPa
Ultimate stress	380 MPa	676 MPa
Failure strain	0.10 ~ 0.60	0.10 ~ 0.60

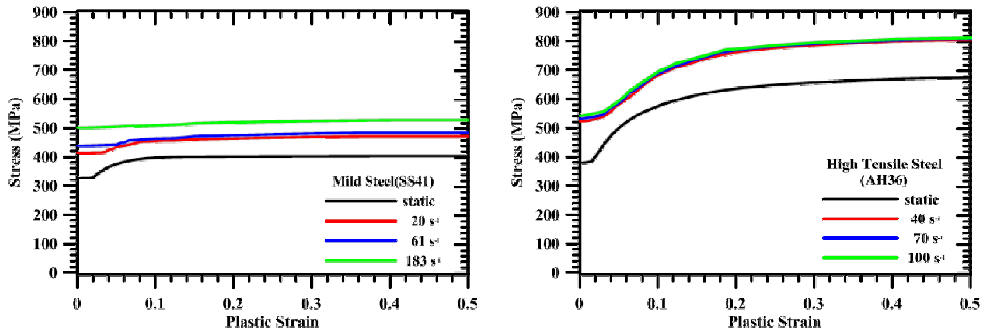

(a) SS41 & AH36 original test s-s curve with curve fitting process

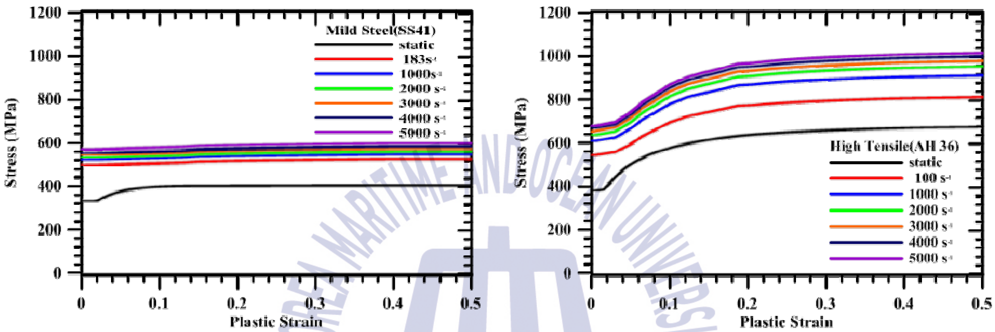

(b) SS41 & AH36 extended s-s curve using Cowper and Symonds model

Fig. 18 Stress-strain curves of mild and high tensile steels with strain rate effect

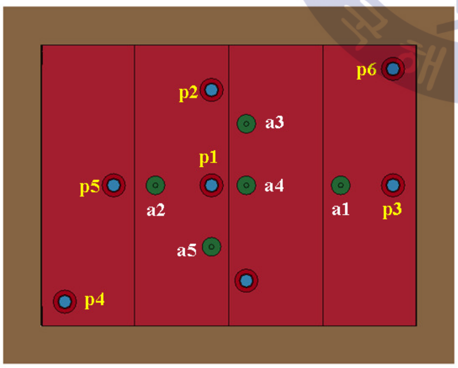

(a) 1st~4th reduced scale BH

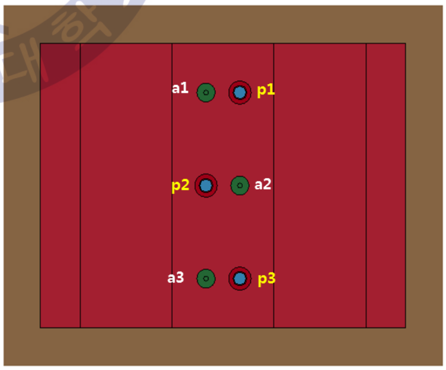

(b) 5th reduced scale BH

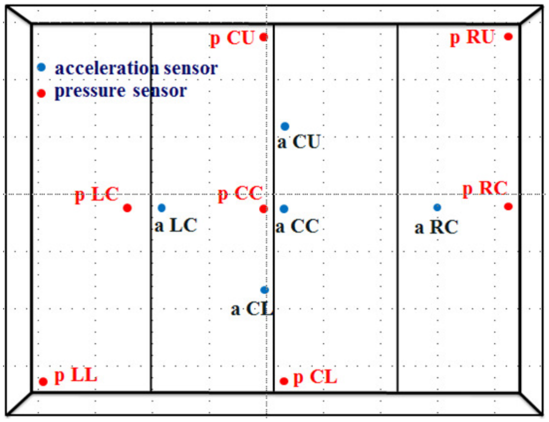

(c) partial chamber BH

Fig. 19 Pressure & acceleration sensor locations on reduced scale & partial chamber bulkheads

4. Shock Response Analysis of Chamber Models

Figure 20 shows the blast flame configuration from the backward opening and side leakage between chamber and bulkhead cartridge in the case of simulation and test of reduced scale chamber model under the internal blast of HE TNT charge, and Fig. 21 shows the propagation process of shock wave at the longitudinal vertical plane in the partial chamber model according to the stand-off distance of HE TNT charge under internal blast. The difference of shock wave propagation to the bulkhead could be figured out well between initial shock wave and reflect wave against the internal chamber wall according to the location of HE TNT charges.

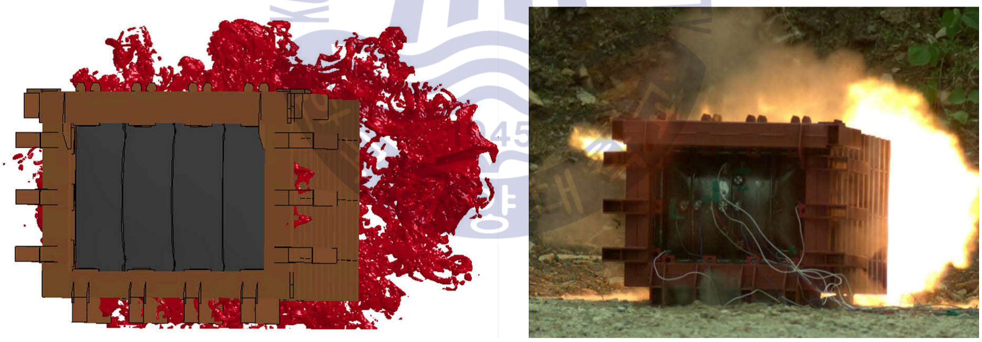

(a) simulation (b) test

Fig. 20 Blast frame in reduced scale chamber model under internal blast of HE TNT charge

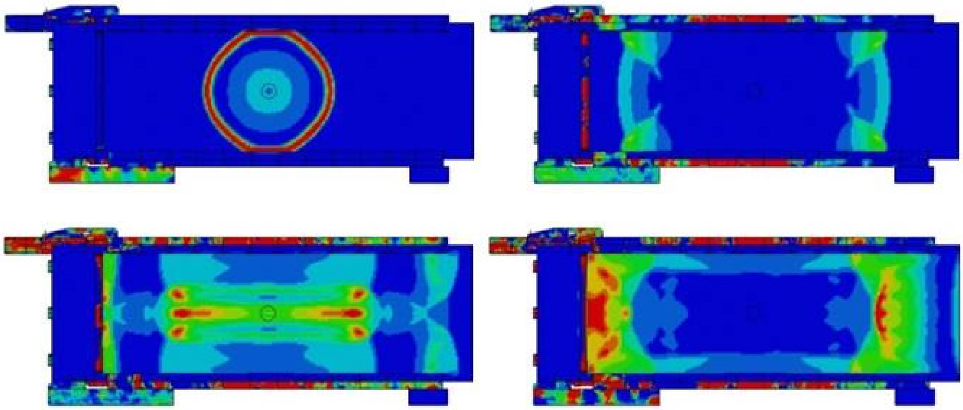

(a) plain & curtain type BH at L/2, HE TNT

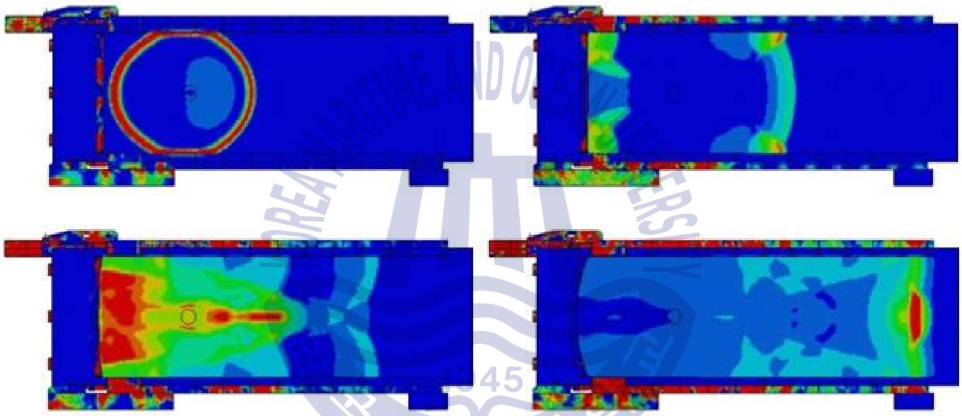

(b) plain type BH at L/4, HE TNT

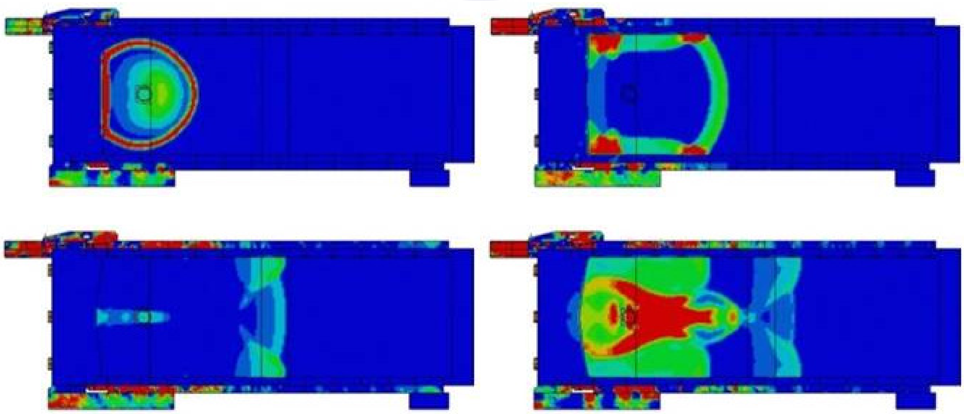

(c) plain type BH at L/8, HE TNT

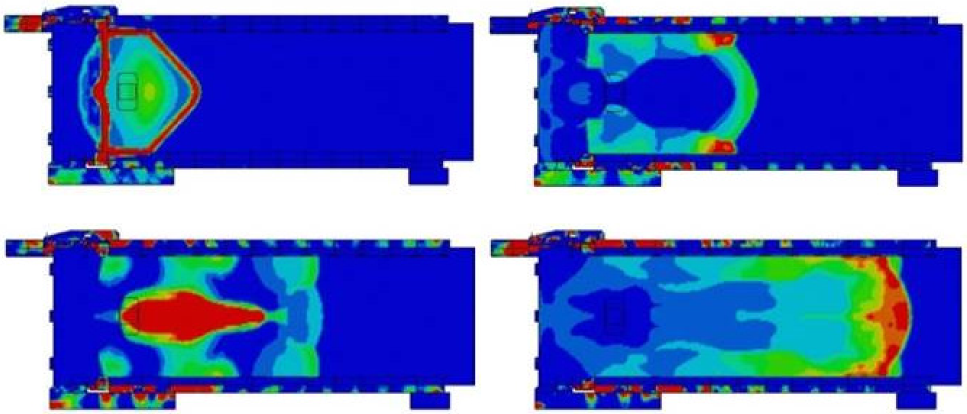

(d) plain type BH at L/16, 2 × HE TNT

Fig. 21 Propagation of shock pressure in part chamber model according to stand-off distance of HE TNT charge

Figure 22 shows the overall maximum stress, plastic strain and deformation response configurations of reduced scale chamber including curtain type bulkhead with HE TNT charge, and Fig. 23, the overall maximum plastic strain distributions of partial chamber including curtain and plain type bulkheads according to stand-off distance with HE TNT charge. Very large responses could be found at the bulkhead compared to the chamber and clamp frames.

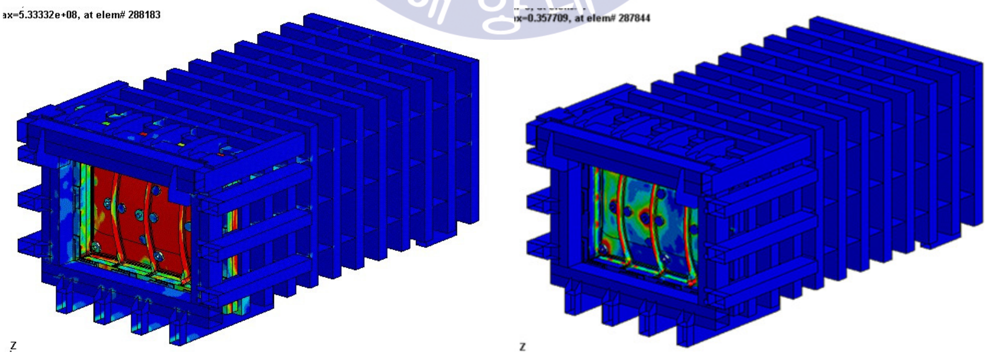

(a) stress (b) plastic strain

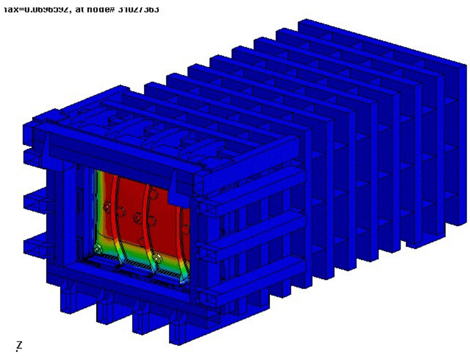

(c) deformation

Fig. 22 Damage response configurations of reduced scale chamber model with HE TNT charge

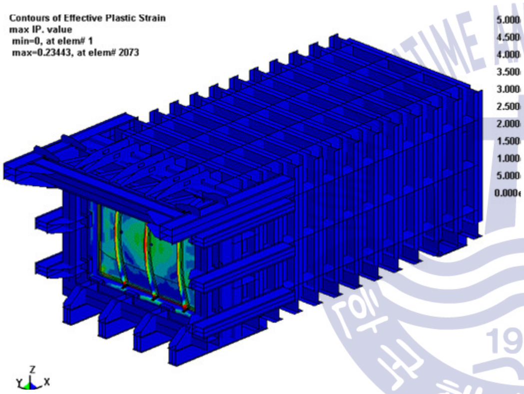

(a) curtain L/2

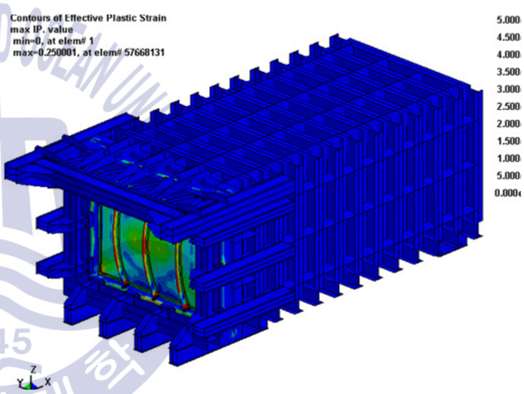

(b) plain L/2

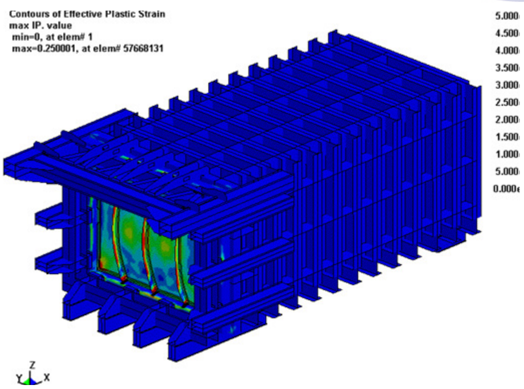

(c) plain L/4

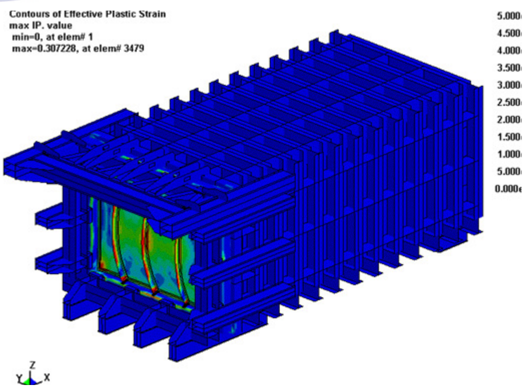

(d) plain L/8

Fig. 23 Plastic strain response configurations of partial chamber model according to stand-off distance of HE TNT charge

Figure 24 shows the damage response configurations in reduced scale chamber bulkhead models, such as plastic strain, under the internal blast simulations of HE TNT charge. From these damage responses, very sharp stress concentration parts and rupture configurations could be found in the bulkhead, stiffeners and cartridge frame, and damage responses, also confirmed to be very sensitive to the welding condition due to the very thin bulkhead plate as shown in the internal blast test results of Fig. 10. The mechanism of the inserted plate to the cartridge could be also found to play a decisive role in deformation and damage in reduced scale chamber bulkhead according to the welding range to the cartridge in the internal blast test and simulation. It could be found that damage configuration of each bulkhead generally shows good agreement with internal blast test result of Fig. 10.

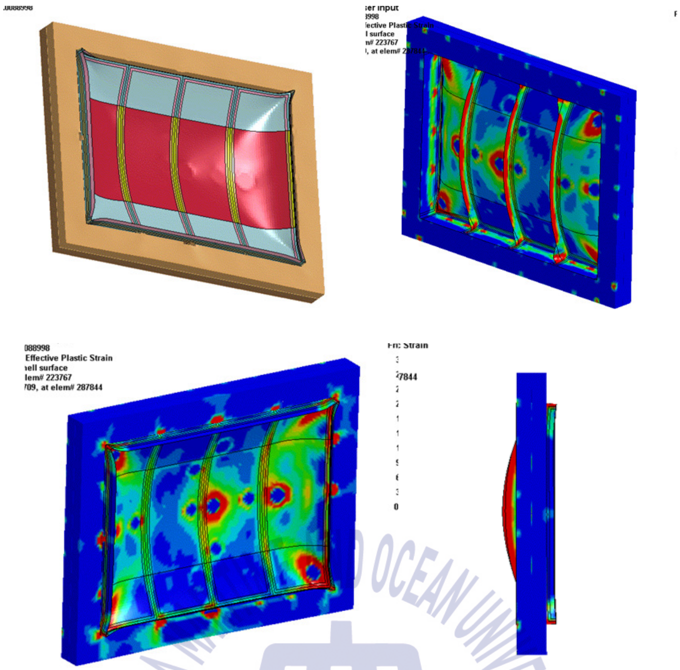

(a) 1st model

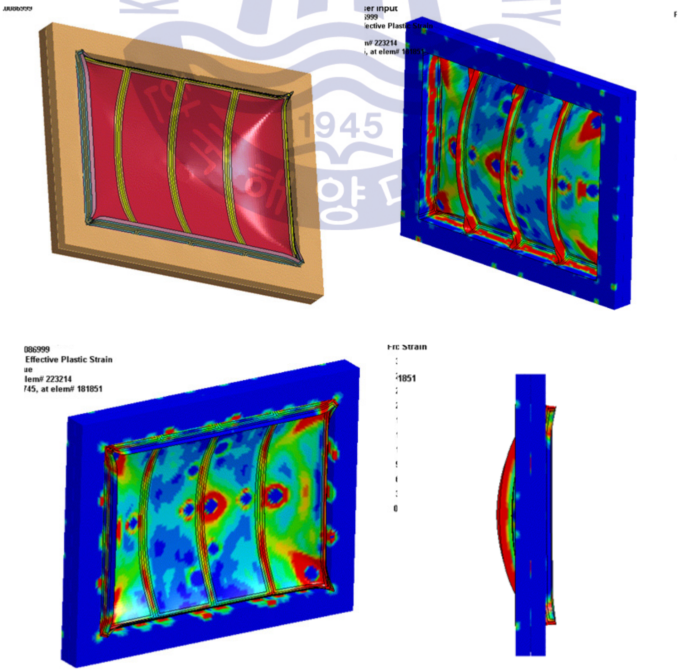

(b) 2nd model

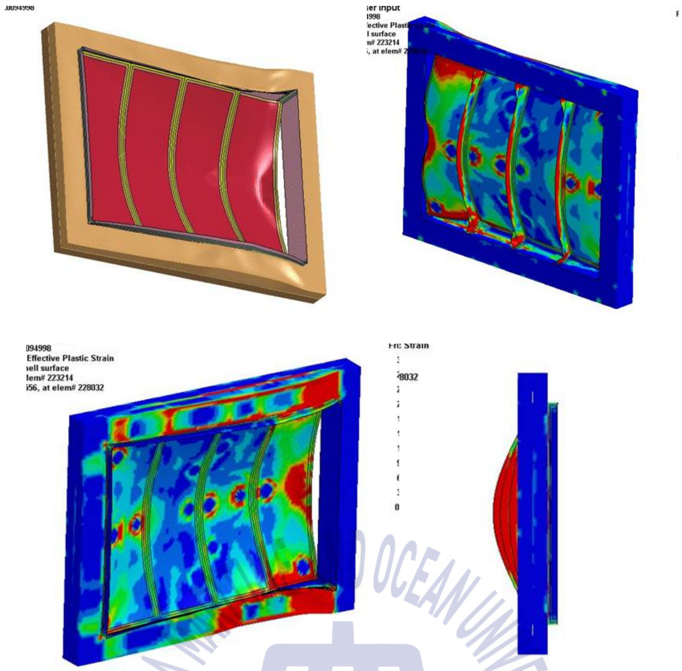

(c) 3rd model

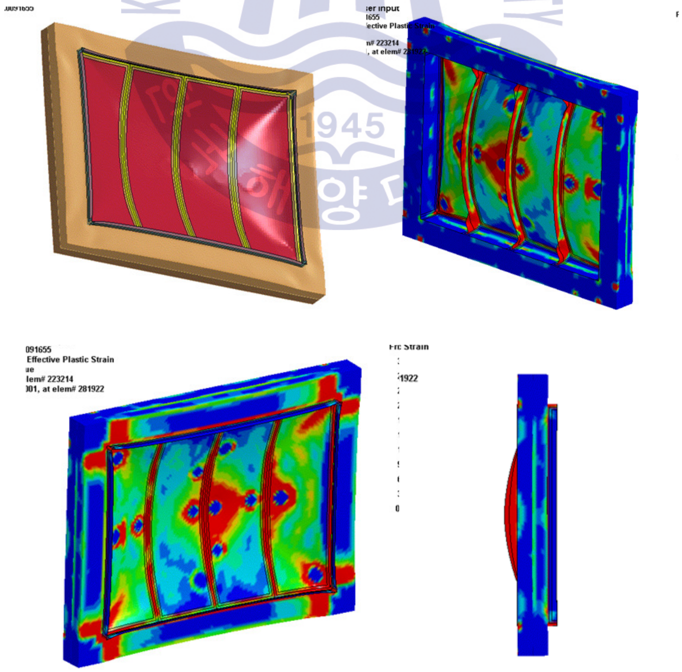

(d) 4th model

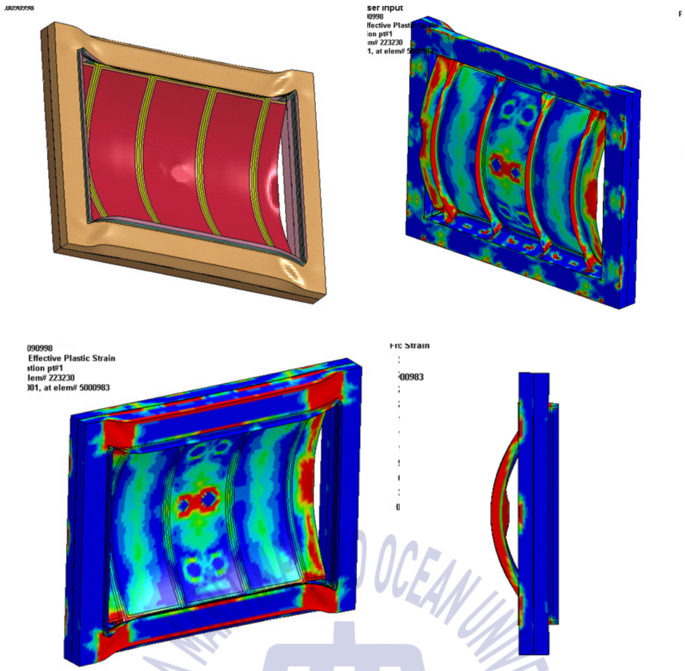

(e) 5th model

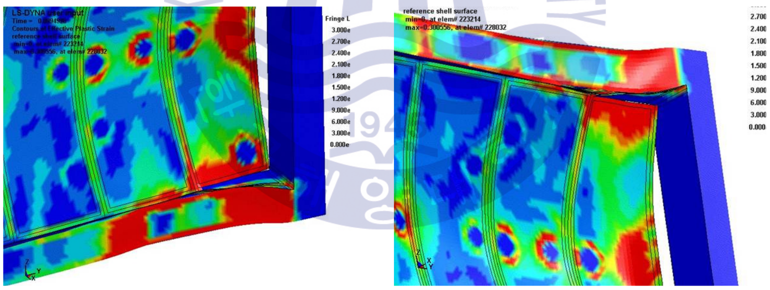

(f) close view of 3rd model

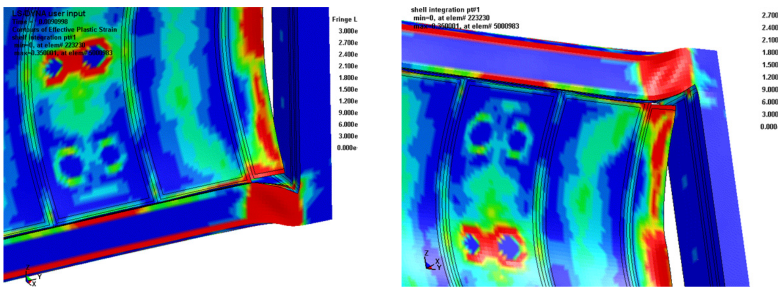

(g) close view of 5th model

Fig. 24 Damage response configurations in reduced scale chamber bulkhead models under internal blast simulation of HE TNT charge

Figures 25 & 26 illustrate the plastic strain and deformation response configurations at the partial chamber curtain and plain type bulkheads according to the stand-off distance HE TNT charge, respectively, and Figs. 27 & 28, their plastic strain responses at the center, corners of bulkhead and the end of stiffeners, and deformation responses along the vertical, horizontal and diagonal directions from the center at the bulkhead for the confirmation of their response according to bulkhead type and stand-off distance HE TNT charge, respectively.

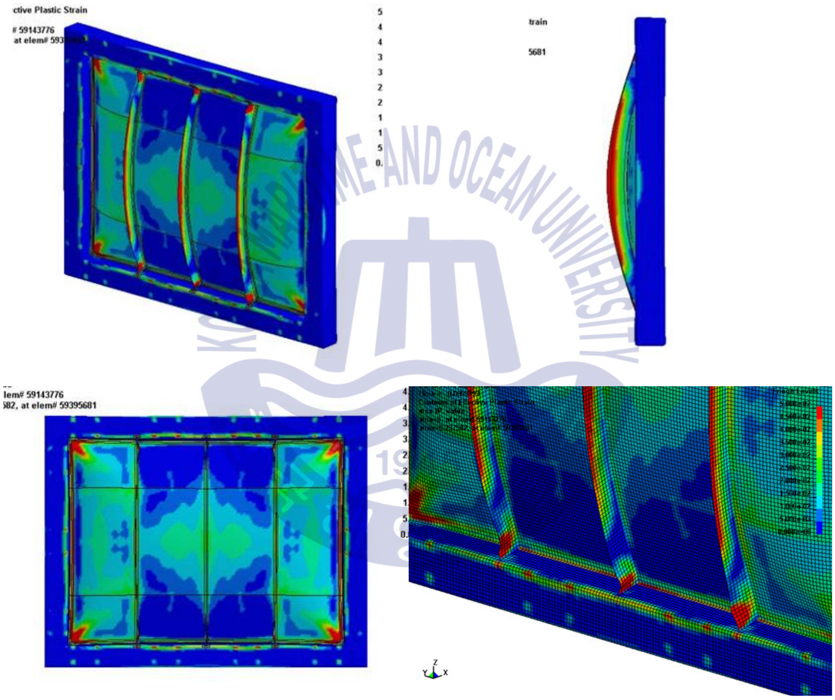

(a) curtain type, L/2 HE

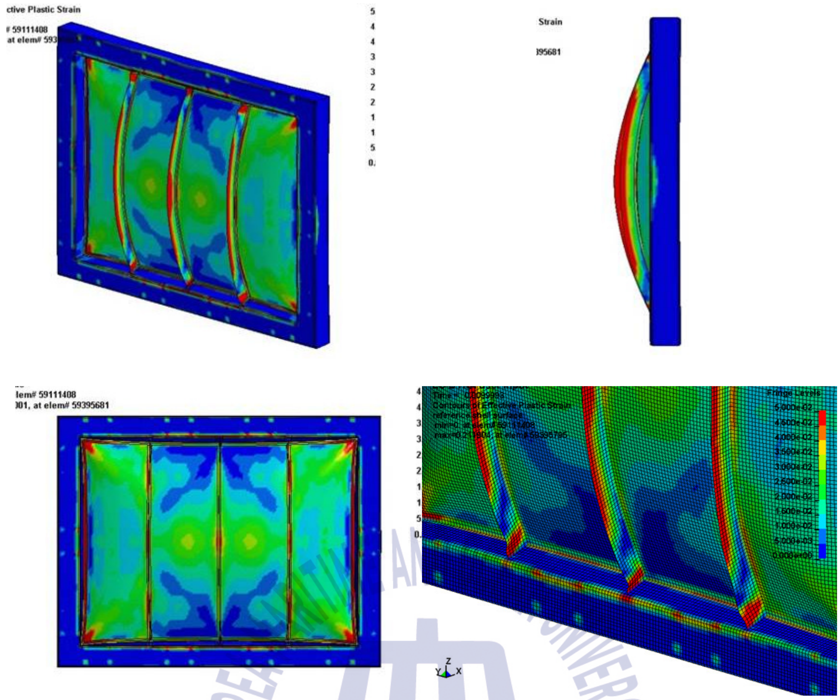

(b) plain type, L/2 HE

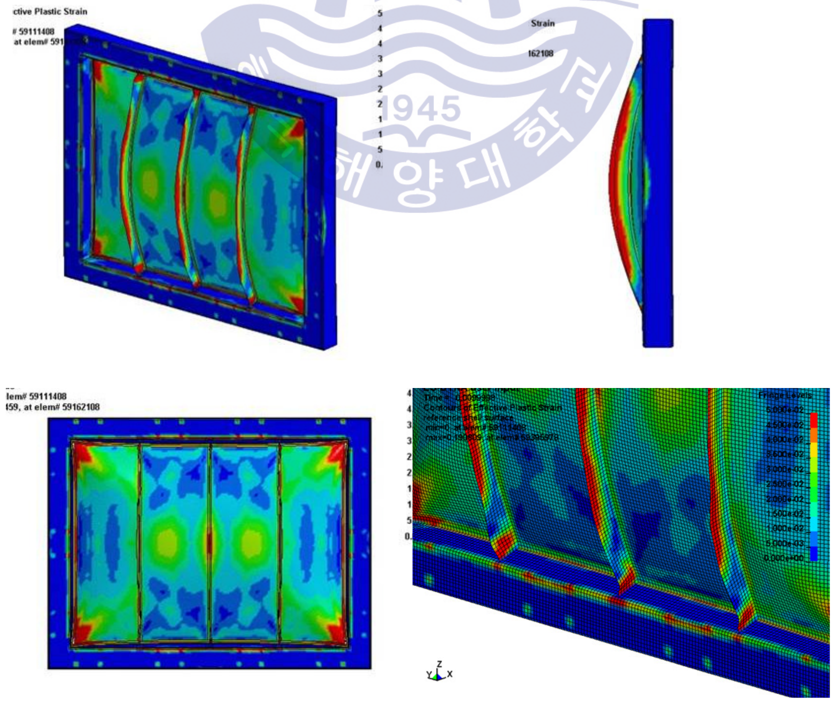

(c) plain type, L/4 HE

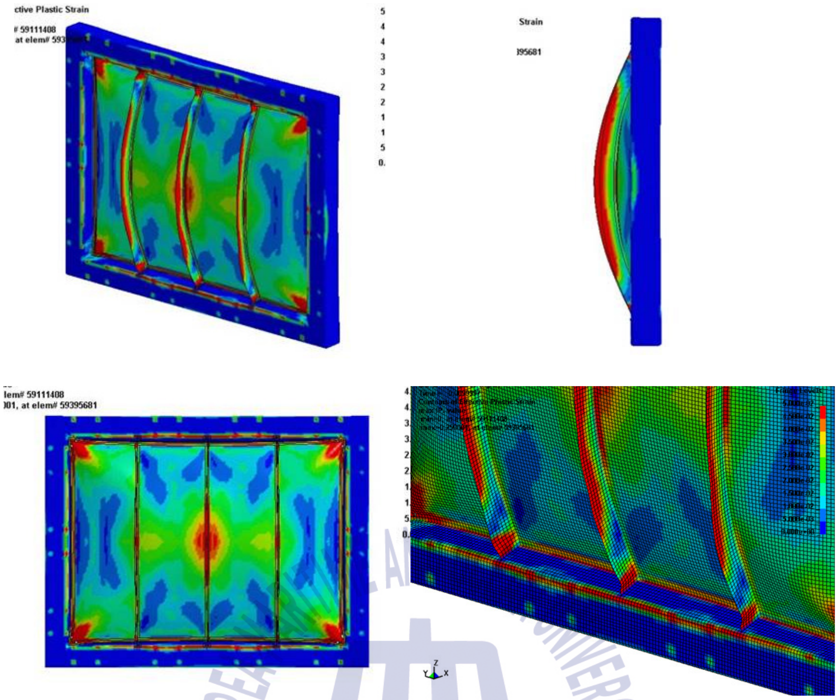

(d) plain type, L/8 HE

Fig. 25 Plastic strain response configurations in partial chamber bulkheads according to stand-off distance of HE TNT charge

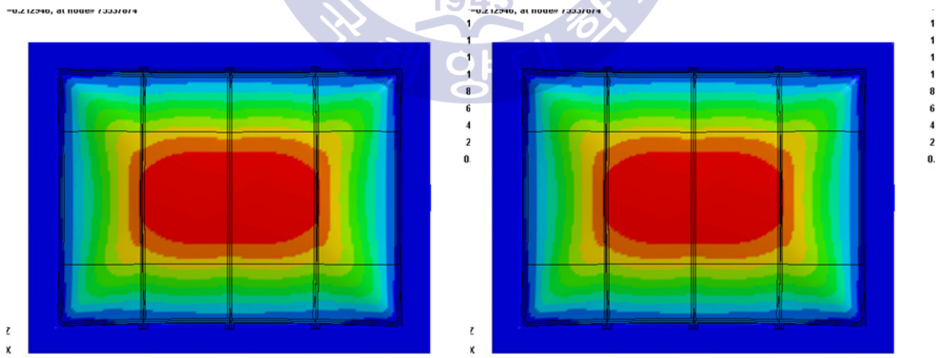

large deformation　　simulation end time

(a) curtain type, L/2 HE

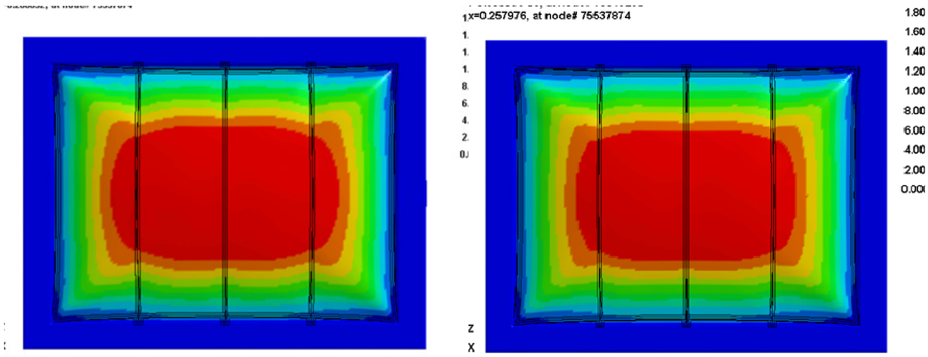

large deformation simulation end time

(b) plain type, L/2 HE

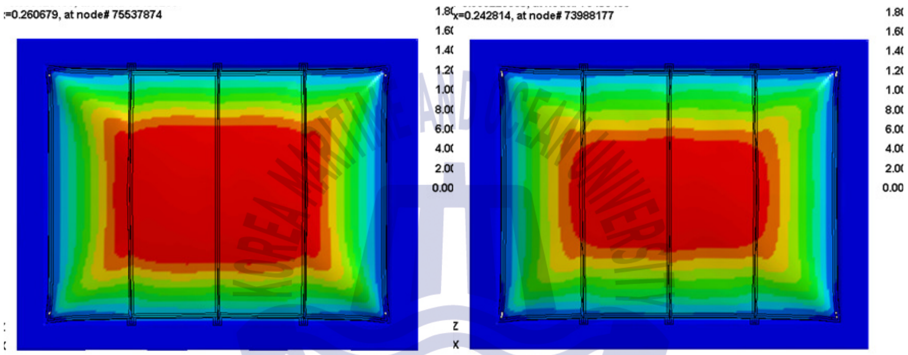

large deformation simulation end time

(c) plain type, L/4 HE

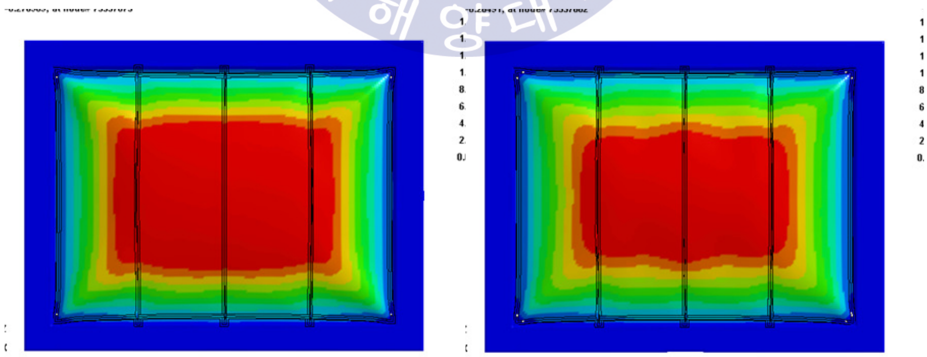

(d) plain type, L/8 HE

Fig. 26 Deformation response configurations in partial chamber bulkheads according to stand-off distance of HE TNT charge

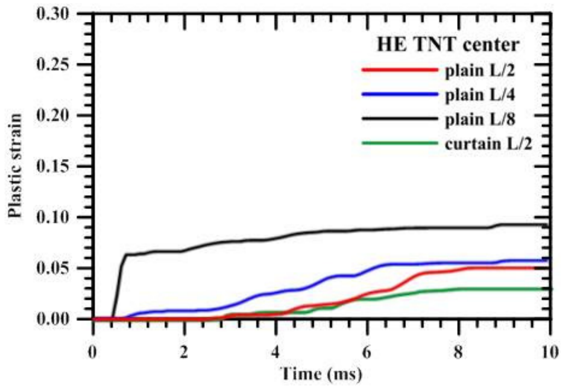

(a) center at BH

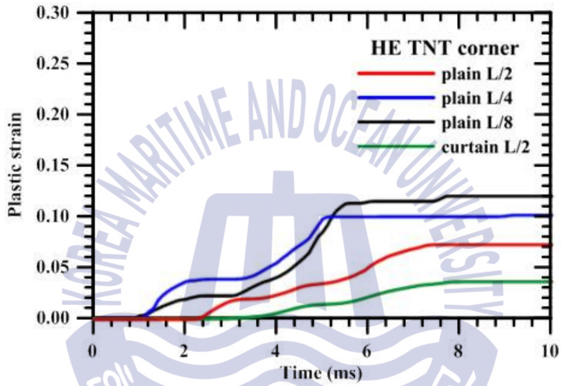

(b) corners at BH

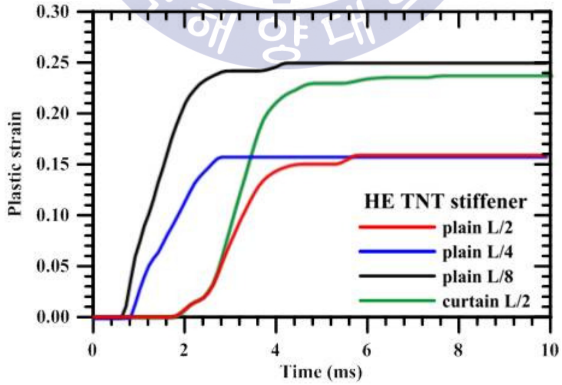

(c) end part at stiffener

Fig. 27 Plastic strain responses in partial chamber bulkheads according to stand-off distance of HE TNT charge

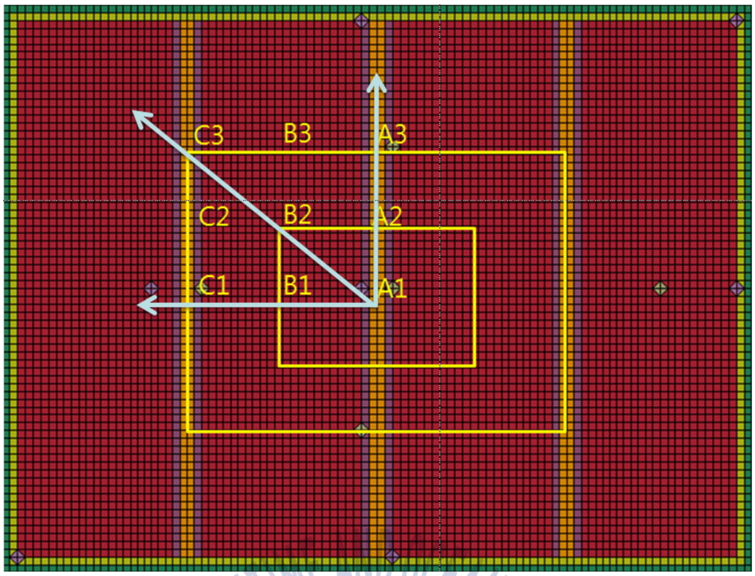

(a) deformation direction

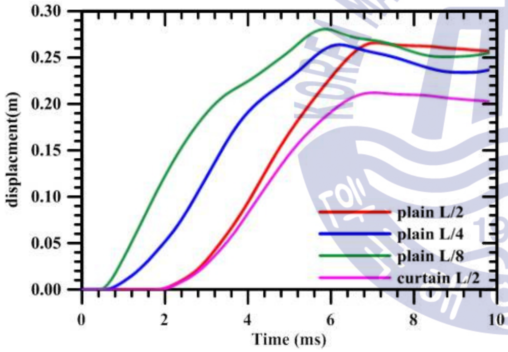

(b) A1

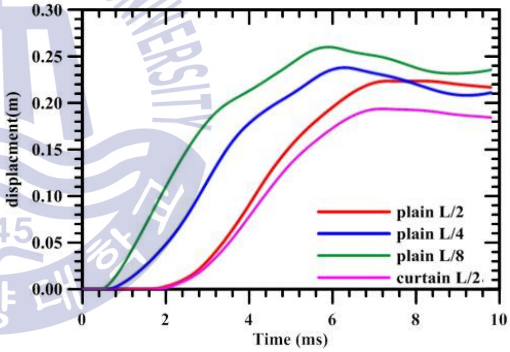

(c) A2

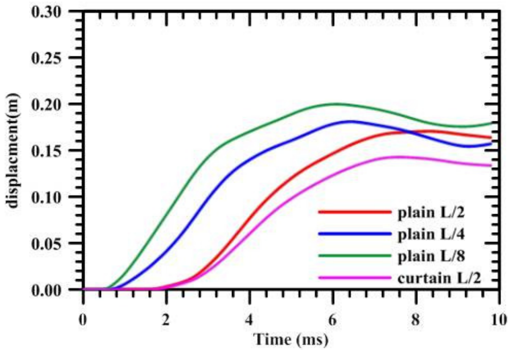

(d) A3

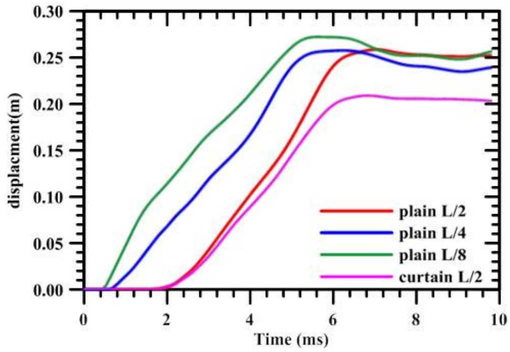

(e) B1

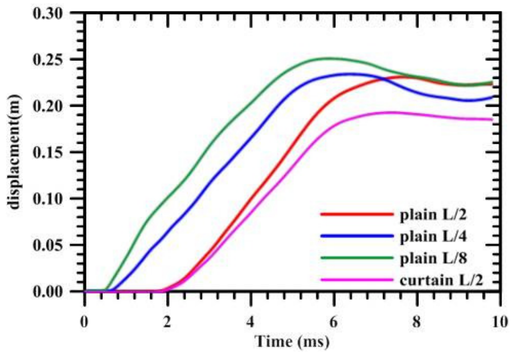

(f) B2

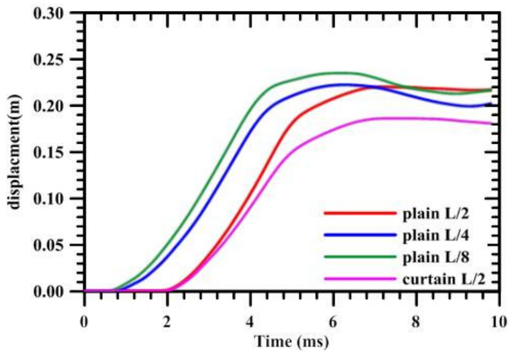

(g) C1

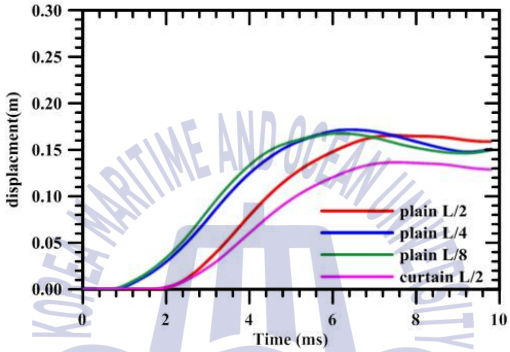

(h) C3

Fig. 28 Deformation responses in partial chamber bulkheads according to stand-off distance of HE TNT charge

As expected, the maximum and range of plastic strain of the plain type bulkhead increased at the center of bulkhead with the decrease of stand-off distance of HE TNT charge to the bulkhead, and large plastic strain also occurred at the corners of bulkhead with the decrease of stand-off distance of HE TNT charge to the bulkhead, since the shock pressure was impacted to the corners by the reflection wave. Those of the curtain type bulkhead occurred relatively smaller than those of the plain type bulkhead at stand-off distance L/2 of HE TNT charge. Very high plastic strain also occurred at the end of stiffeners next to the welding bead together with buckling phenomena because of compression, and the same trends appeared as the center and corners of bulkhead according to stand-off distance of HE TNT charge and bulkhead type. However, there was no rupture in every bulkhead including stiffeners in the bulkhead type and stand-off distance of HE TNT charge. The plain type bulkhead generally deformed larger and more widely compared to the curtain type one. Unexpectedly, deformation magnitude and range at the plain type bulkhead were not increased linearly according to the decrease of stand-off distance of HE TNT charge to the bulkhead, and they were decreased and increased again as the stand-off distance of HE TNT charge from L/2, L/4 and L/8, as shown in Figs. 26 & 28, which might be due to the reflection wave to the corners.

In the case of the curtain type bulkhead with reversed direction at the stand-off distance L/2 of HE TNT charge, stiffeners buckled and their only end parts were torn away in the neighbor layer near welding bead in the internal blast simulation and test, as shown in Figs. 11(b) & 29. Very close internal blast simulation results are shown in Fig. 30, and the whole bulkhead was torn away from the bulkhead bead attached in cartridge and most upper and bottom cartridge part, also, along the bulkhead welding line with broken concrete, as shown in Fig. 12. Very huge velocities could be found at the center, mid points of upper and side at bulkhead in the internal blast simulation, as shown in Fig. 30. Fracture criterion could be set up for this internal blast simulation considering welding effects.

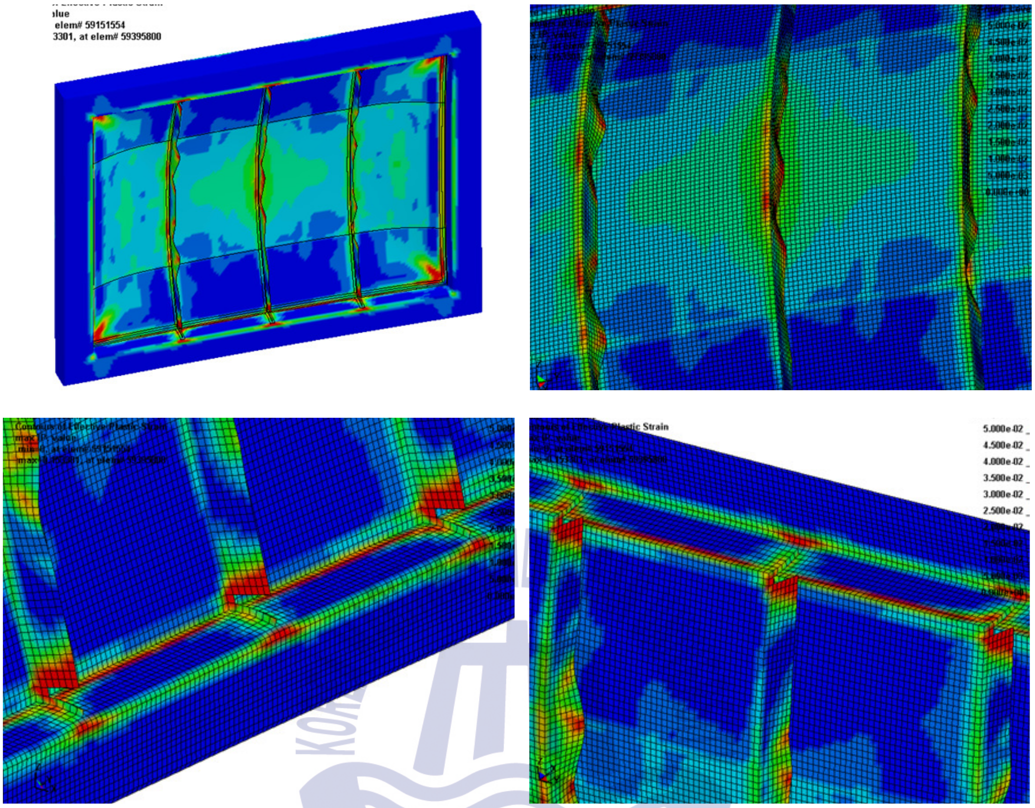

Fig. 29 Damage configurations of curtain type partial chamber bulkhead under HE TNT charge with reversed direction and stand-off distance L/2

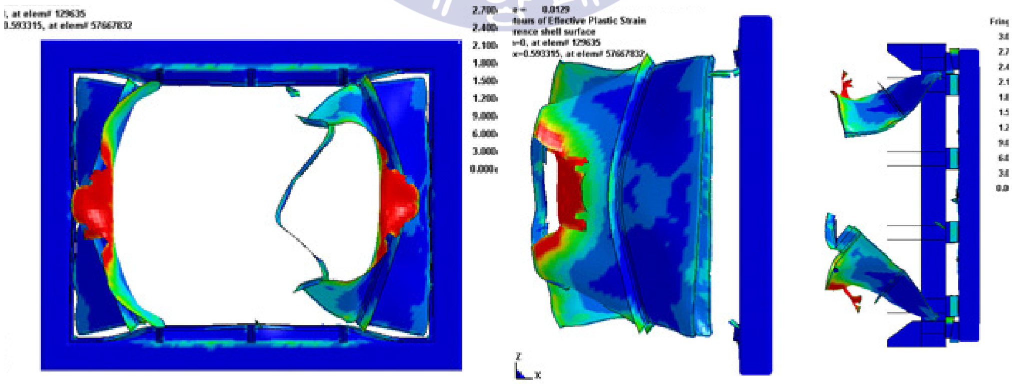

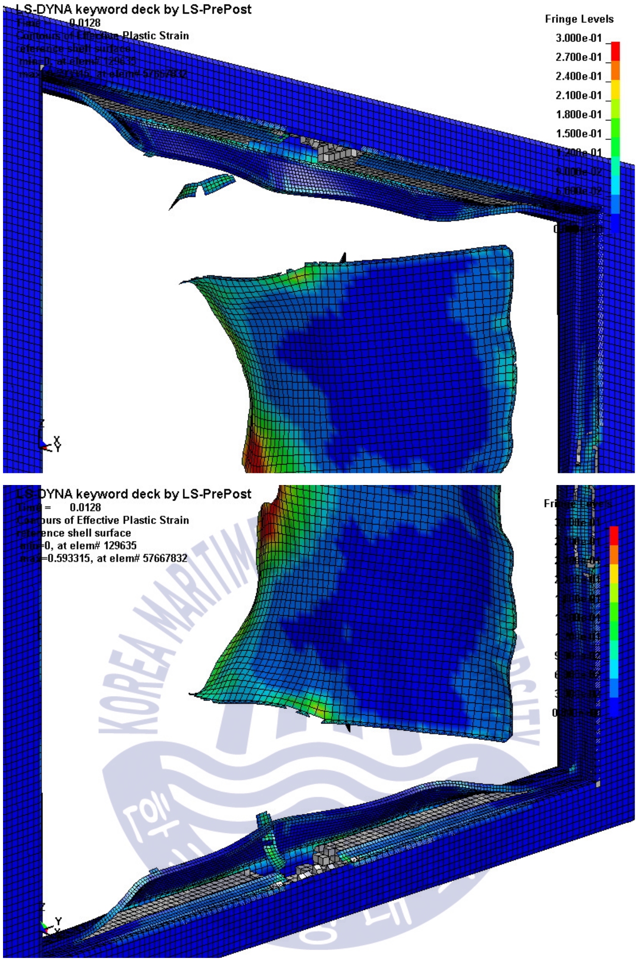
LS-DYNA keyword deck by LS-PrePost
Time = 0.0128
Contours of Effective Plastic Strain
reference shell surface
min=0, at elem# 129635
max=0.593315, at elem# 57667832
Fringe Levels
3.000e-01
2.700e-01
2.400e-01
2.100e-01
1.800e-01
1.500e-01

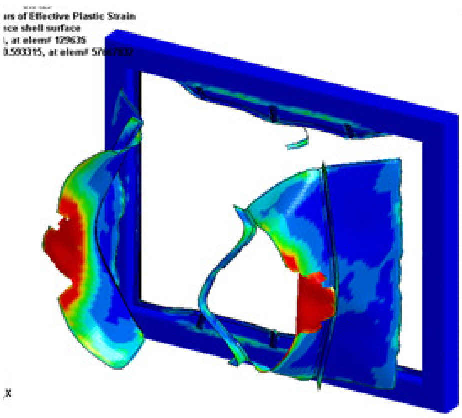

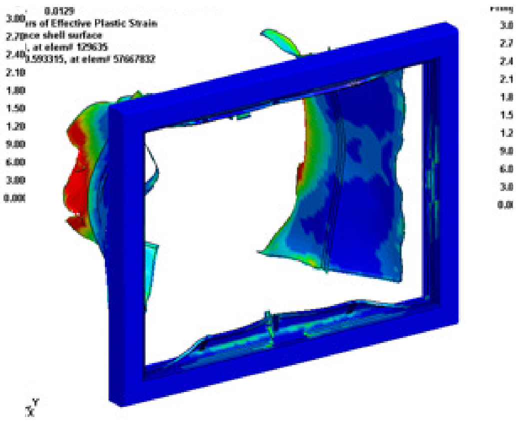

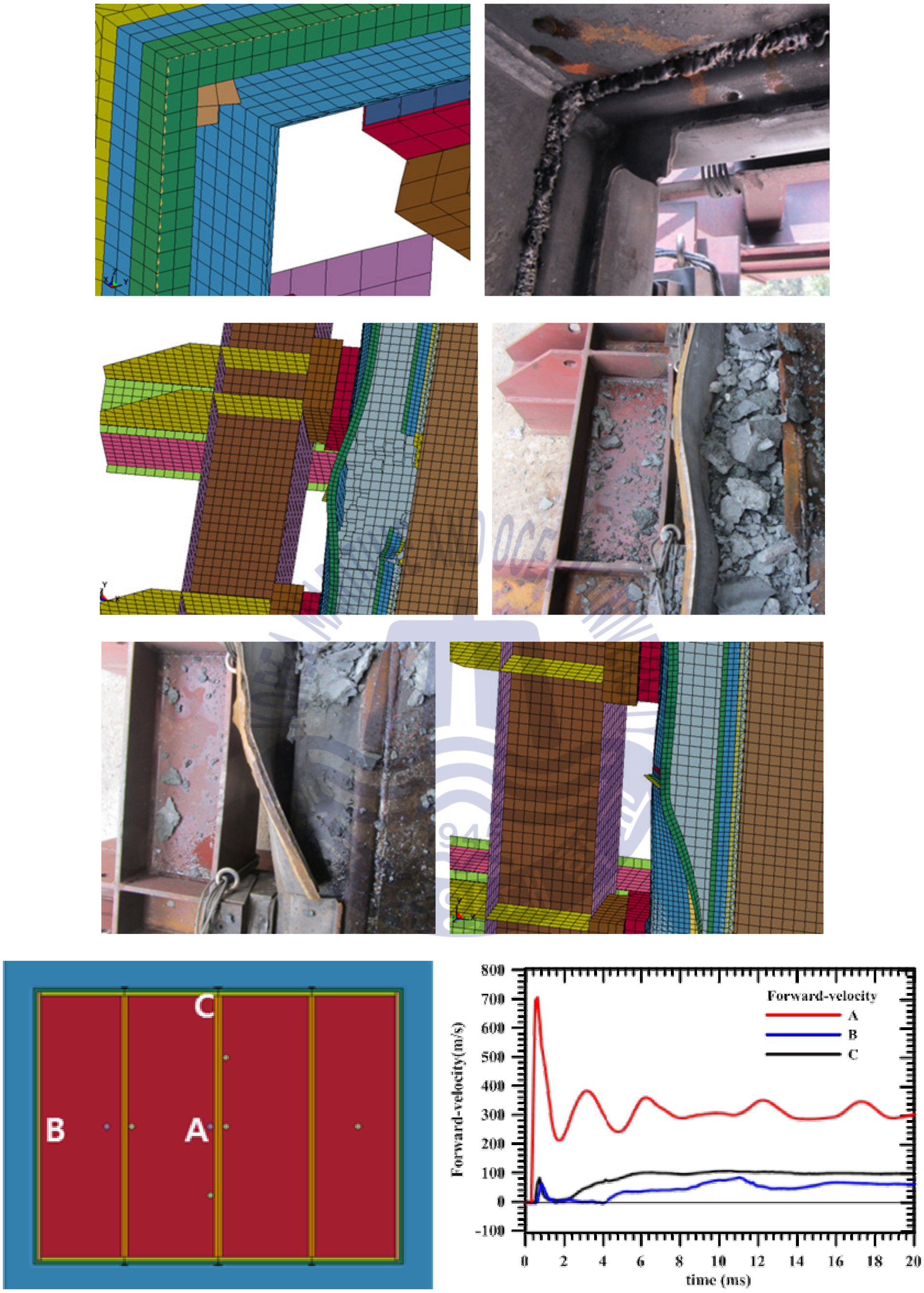

Fig. 30 Damage configurations of plain type partial chamber bulkhead under 2 × HE TNT charge at stand-off distance L/16

Responses could not be measured fully correctly in the first internal blast test using the 1st~3rd reduced scale chamber models, with only some pressure ones of the 2nd one. Both pressure and acceleration responses of the 4th and 5th models were measured at the locations of bulkhead, as shown in Fig. 19(a)~(b), and compared to those of test with HE TNT charge, as shown in Figs. 31~34, respectively. All responses are represented by the non-dimensional scale. It could be found that the pressure and acceleration responses generally show good agreement with those of internal blast test

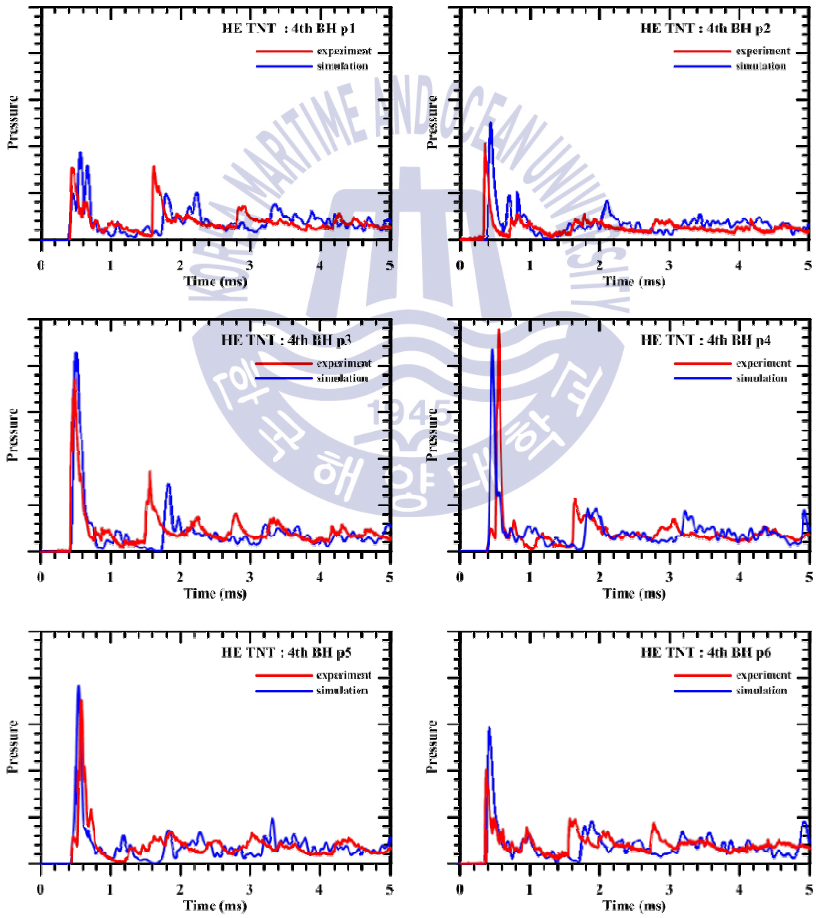

Fig. 31 Pressure responses between experiment & simulation with HE TNT at 4th bulkhead

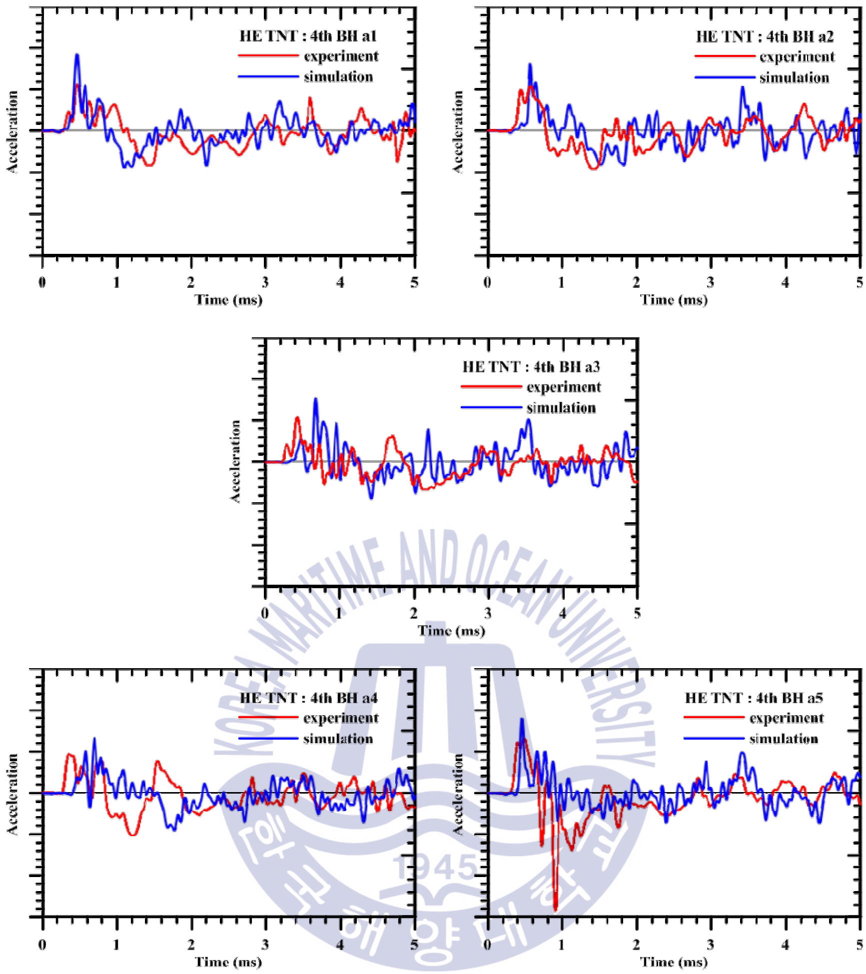

Fig. 32 Acceleration responses between experiment & simulation with HE TNT at 4th bulkhead

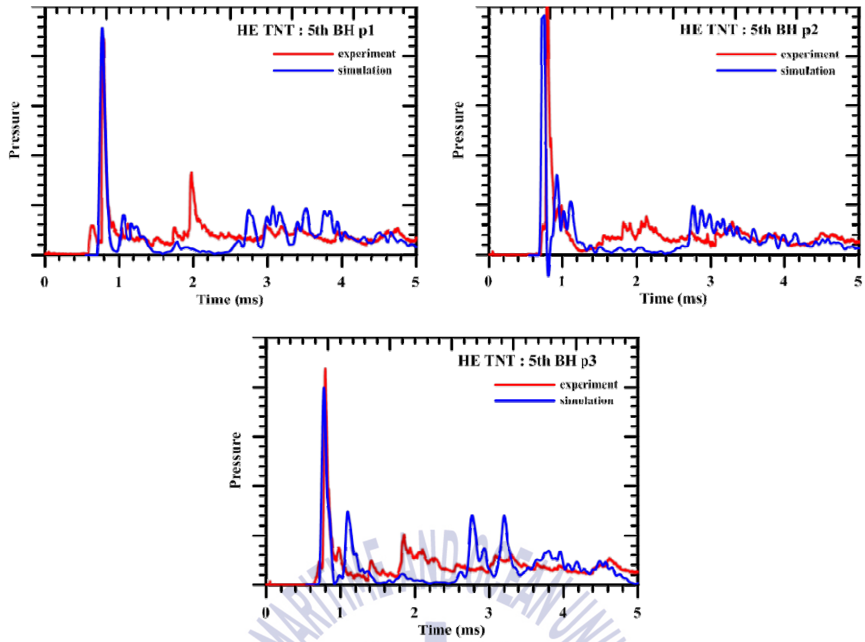

Fig. 33 Pressure responses between experiment & simulation with HE TNT at 5th bulkhead

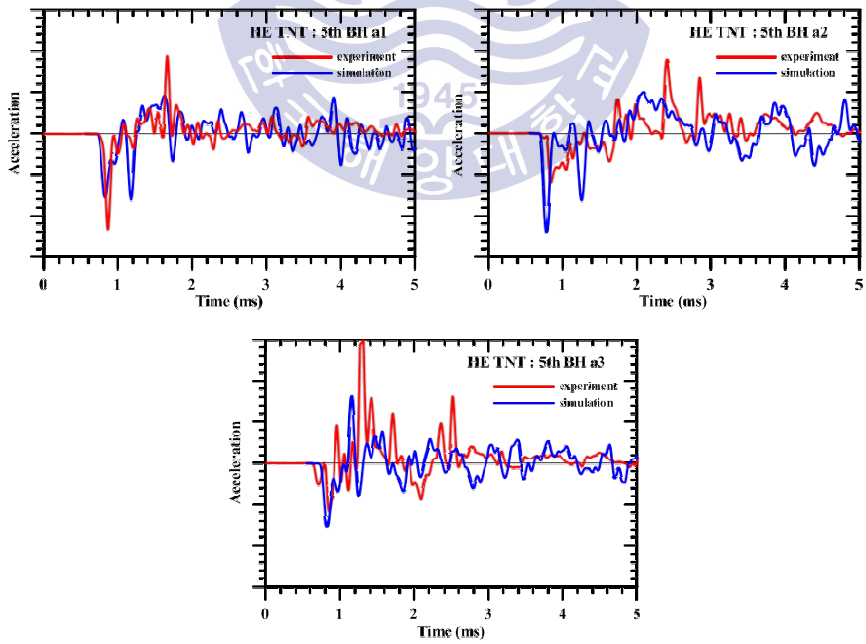

Fig. 34 Acceleration responses between experiment & simulation with HE TNT at 5th bulkhead

Pressure and acceleration responses were measured at the locations of bulkhead, as shown in Fig. 19(c). Among the whole internal blast test of partial chamber models, pressure and acceleration responses of plain type bulkhead at stand-off distance L/2 & L/4 and curtain one at stand-off distance L/2 were typically compared to those of internal blast tests, as shown in Fig. 35~40. It could be also found that the pressure and acceleration responses generally show good agreement with those of internal blast test, as the case of reduced scale chamber models.

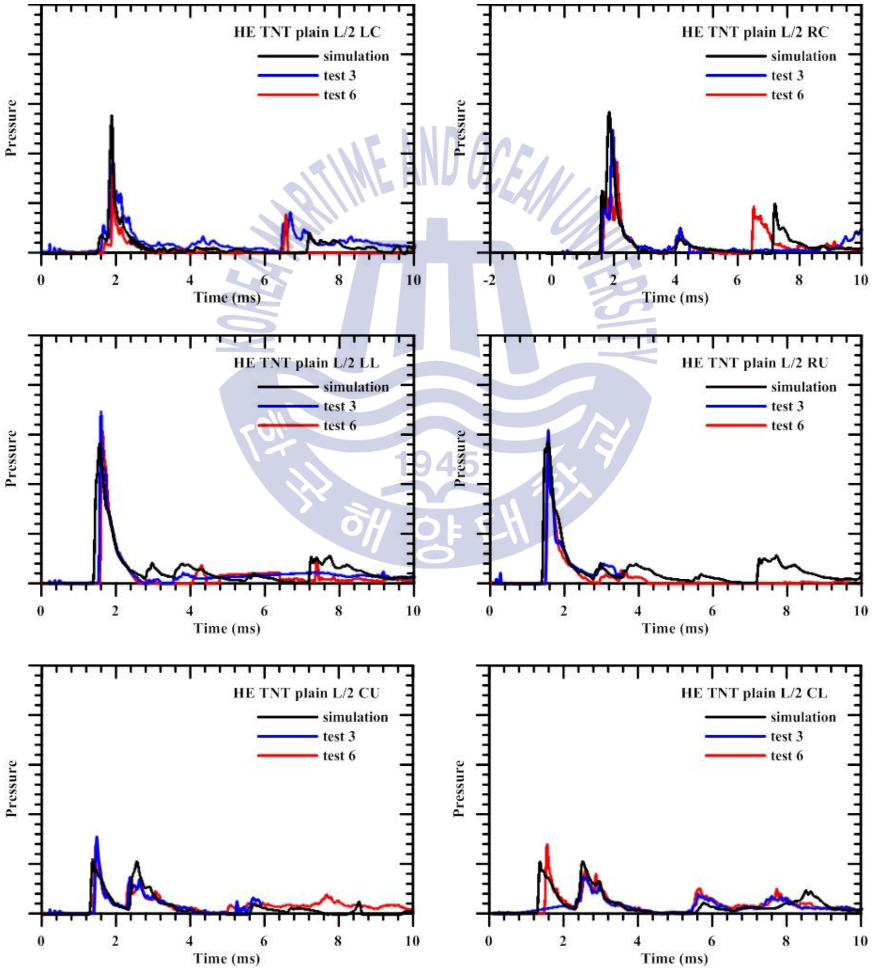

Fig. 35 Pressure responses between experiment & simulation with HE TNT in plain type bulkhead at stand-off distance L/2

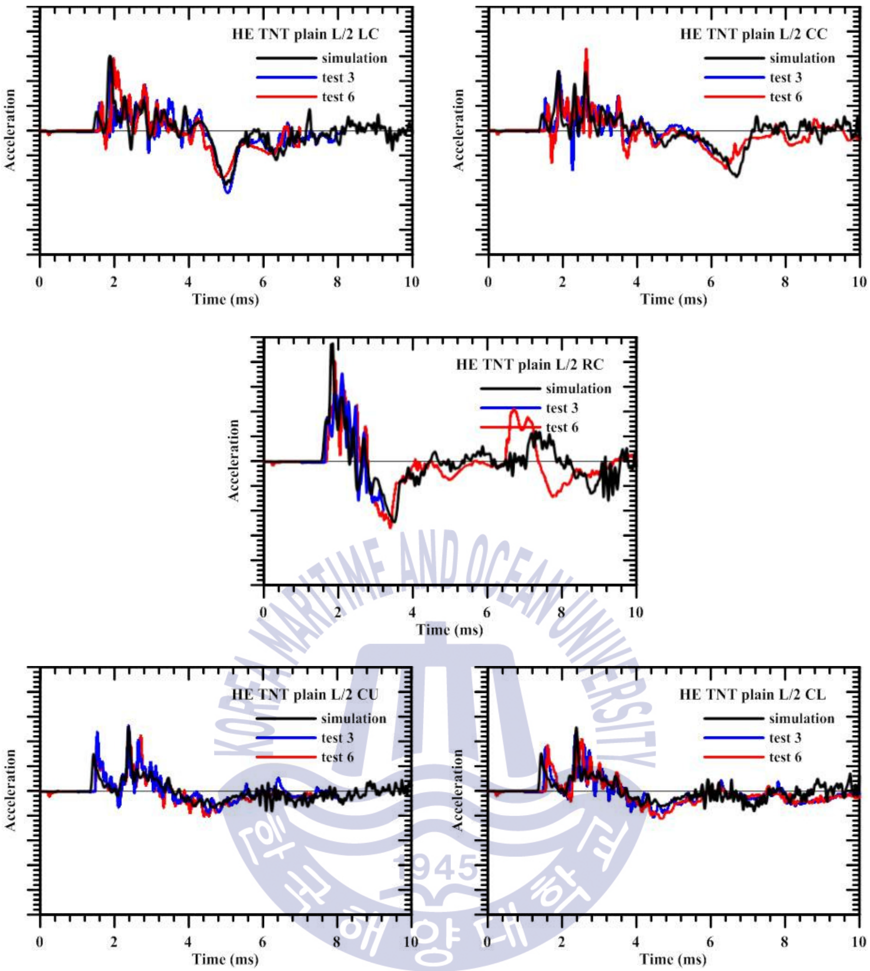

Fig. 36 Acceleration responses between experiment & simulation with HE TNT in plain type bulkhead at stand-off distance L/2

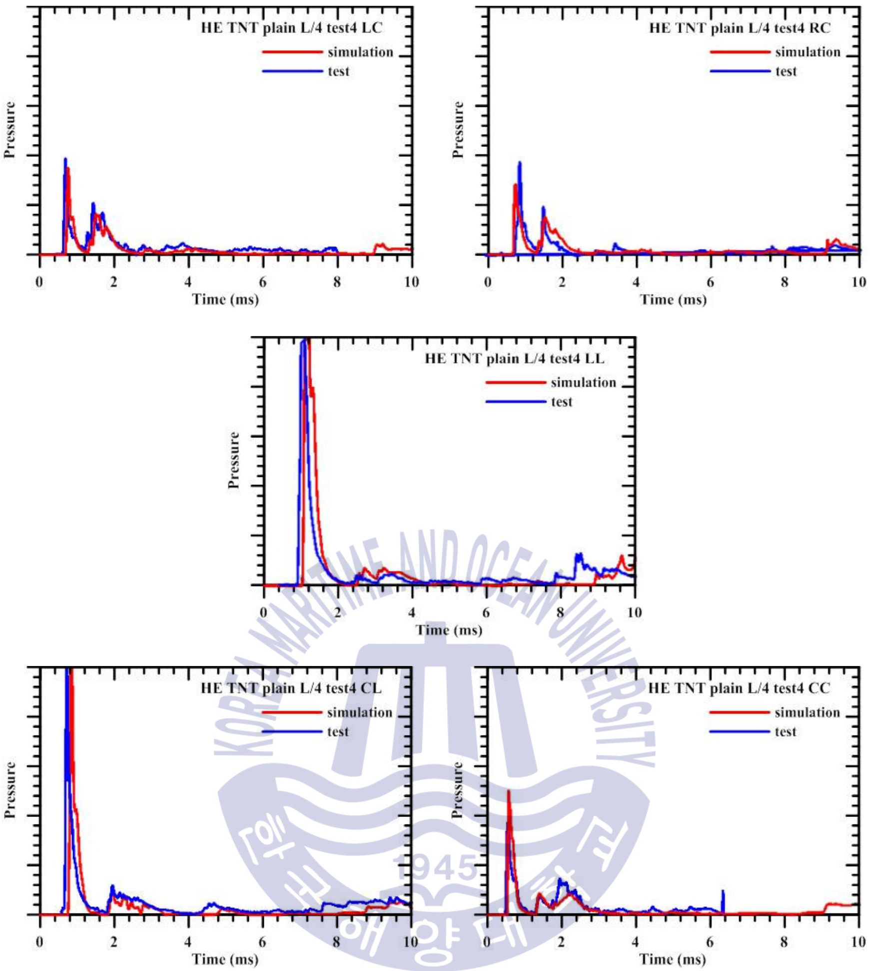

Fig. 37 Pressure responses between experiment & simulation with HE TNT in plain type bulkhead at stand-off distance L/4

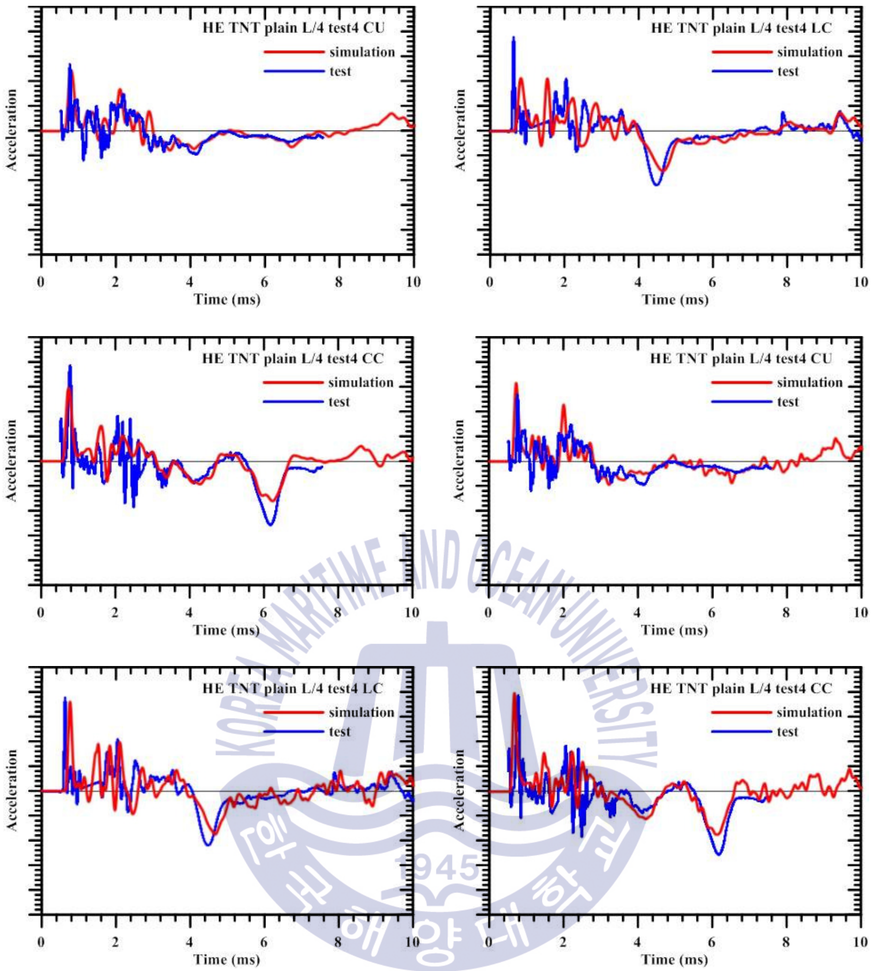

Fig. 38 Acceleration responses between experiment & simulation with HE TNT in plain type bulkhead at stand-off distance L/4

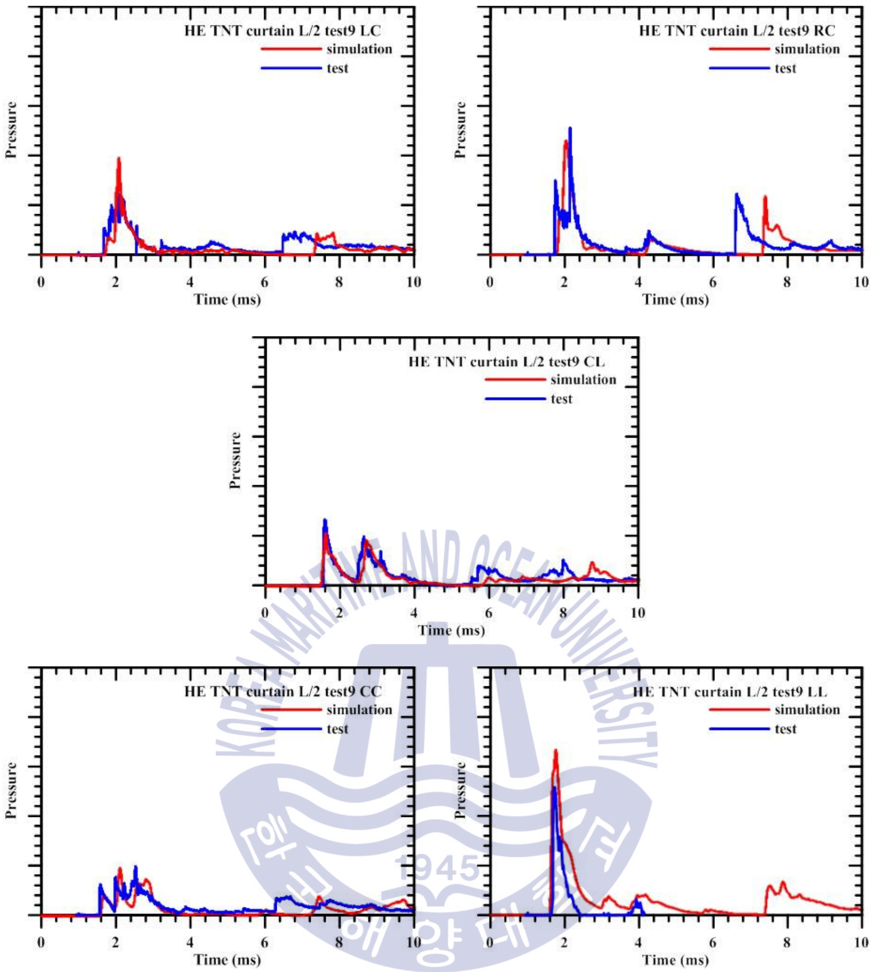

Fig. 39 Pressure responses between experiment & simulation with HE TNT in curtain type bulkhead at stand-off distance L/2

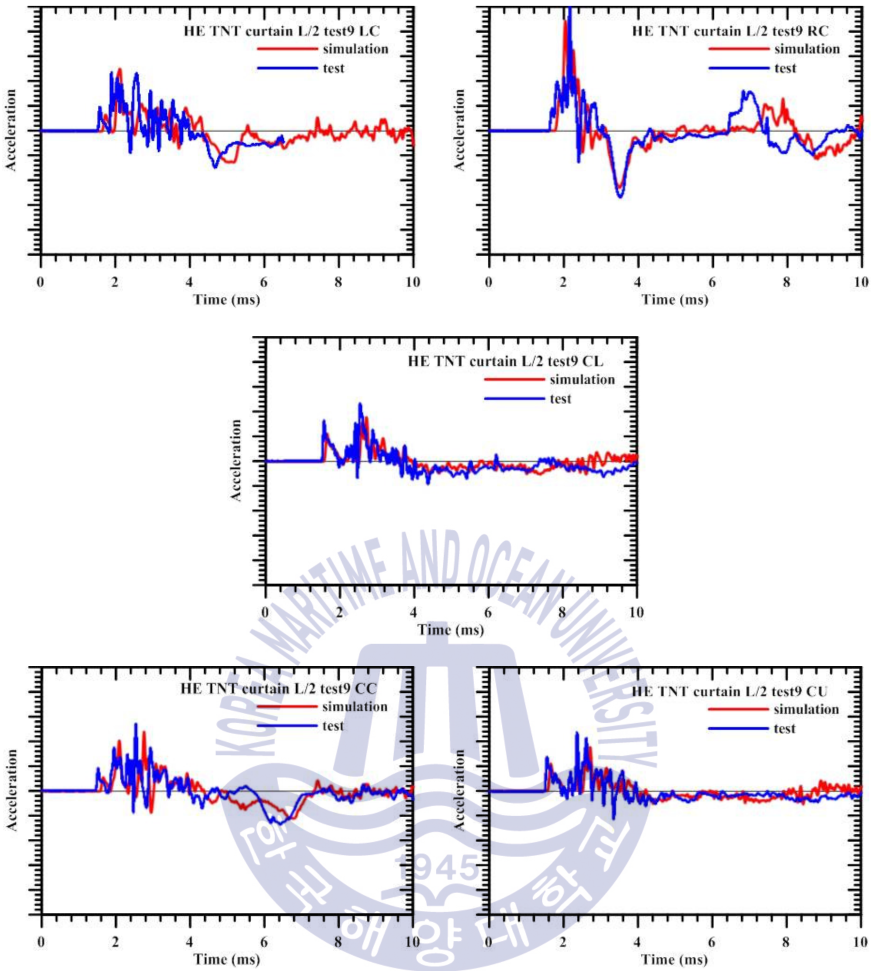

Fig. 40 Acceleration responses between experiment & simulation with HE TNT in plain type bulkhead at stand-off distance L/2

4. Conclusion

In this study, shock response analysis was carried out for the reduced scale and partial chamber models under the internal blast, and its response analysis technique was verified with the test results of 5 bulkhead models of reduced scale chamber models and 2 types of bulkheads of partial chamber ones according to stand-off distance of HE and LE TNT charges, using MMALE formulation and FSI analysis technique of LS-DYNA code. Shock response characteristics could be also figured out through the verifications of response analysis technique compared with the internal blast test results.

Through the verifications of the internal blast simulations with test results, important factors should be considered carefully, such as FSI analysis techniques, damage mechanism, fracture criterion, and welding effects. It could be found that damage configurations of each bulkhead generally showed good agreement with those of internal blast tests, and that pressure and acceleration responses of shock response analysis, also with those of tests.

References

Aquelet, N., Souli, M., & L, Olovsson., 2006. Euler-Lagrange coupling with damping effects: Application to slamming problems, *Computer Methods in Applied Mechanics and Engineering*, 195, pp. 110~132.

Galle, L.F., Erkel. & van A.G., 2002. TNO-PML Developments of Blast Resistant Doors and Wall. *The 1st European Survivability Workshop*, Cologne, Germany.

LSTC, 2013. LS-DYNA User's Manual, Version R7, *Livermore Soft Technology Corp*, USA.

Raymond, I.K., 2012. Tools for the formation of optimized X-80 Steel Blast Tolerant transverse bulkheads. *Master of Engineering Thesis in the University of New South Wales.*

Stark, S. & Sajdak, J., 2012. Design and Effectiveness Criteria for Blast Hardened Bulkhead Applications on Naval Combatants. *The 4th International Conference on Design and Analysis of Protective Structures*, Jeju, Republic of Korea.

Acknowledgement

학부생 4학년 때부터 졸업하기까지 저에게 인생에 도움이 되는 교육과 조언을 위해 항상 시간을 내어주신 이상갑 교수님께 존경을 표합니다. 부족한 저를 위해 잘못된 점을 아낌없이 지적해주시고, 제가 올바른 길을 걸어갈 수 있도록 지도해주셔서 진심으로 감사드립니다.

또한 본 논문을 위해 심사와 조언을 해주신 박석주 교수님과 남종호 교수님께 감사드리며, 6년의 학사과정과 석사과정동안 저에게 많은 도움을 주신 조선해양시스템공학부 교수님들께도 감사드립니다.

제가 석사과정을 시작할 때부터 지금까지 저에게 많은 가르침을 주시고, 어렵고 힘든 일이 있을 때마다 저에게 방향을 제시해주고, 해결방법을 가르쳐주신 재석이형에게 감사를 드립니다. 그리고 저와 같이 석사과정을 하는 지훈이형, 태영이가 있어서 많은 도움이 되었고, 앞으로 남은 과정 또한 열심히 노력하여 좋은 결과가 있기를 바랍니다. 같이 석사과정을 시작하여 지금까지도 좋은 조언을 해주시는 조재상 씨에게도 고마움을 전합니다. 또한 같은 실험실이 아니더라도 힘든 일이 있을 때 조언과 걱정을 아낌없이 해준 조선해양시스템공학부 내의 모든 동기들과 선후배님들에게도 감사하다는 말을 전합니다.

지금이 끝이 아닌 시작이라고 생각하고 앞으로도 저의 부족한 점을 알고 그곳을 채우기 위해 열심히 사는 사람이 되겠습니다. 마지막으로 지금까지 저를 믿어주시고, 기도와 사랑으로 보살펴주신 부모님과 친척가족들에게도 감사드립니다.

본 논문은 방위사업청과 국방과학연구소의 지원으로 수행된 연구의 일부분입니다. 이에 감사의 말씀을 드립니다.